iScience

CellPress
OPEN ACCESS

Article

Many-objective bi-level energy scheduling method for integrated energy stations based on power allocation strategy

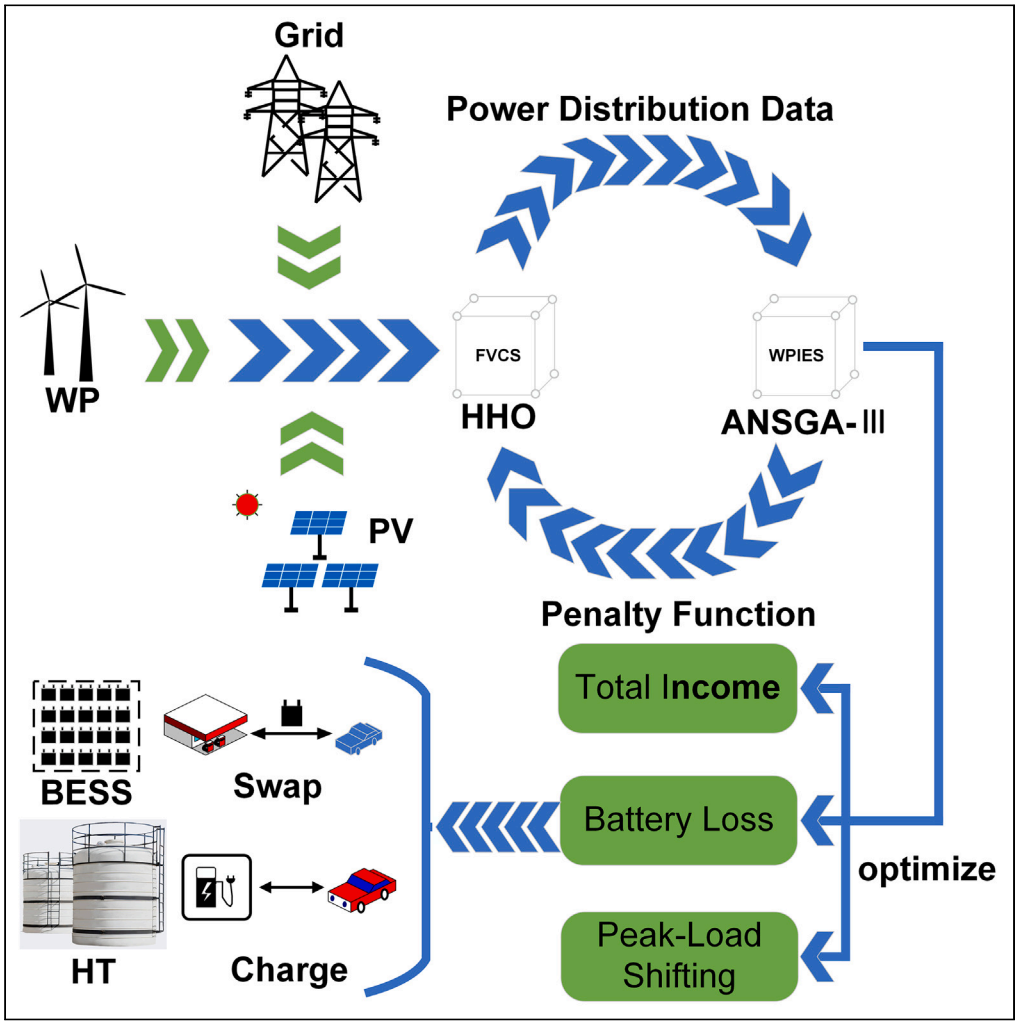

Xiang Liao, Jun Ma, Bangli Yin, Beibei Qian, Runjie Lei, Fu B, Chaoshun Li

ma.jun@hbut.edu.cn

Highlights

The future value competition strategy is proposed to optimize the efficiency of energy use

The optimal scheduling model of WP/PV integrated energy station is proposed

A bi-level optimization model of FVCS-WPIES is proposed

Liao et al., iScience 27, 109305
March 15, 2024
https://doi.org/10.1016/j.isci.2024.109305

iScience

CellPress
OPEN ACCESS

Article

Many-objective bi-level energy scheduling method for integrated energy stations based on power allocation strategy

Xiang Liao,[1] Jun Ma,[1,3,*] Bangli Yin,[1] Beibei Qian,[1] Runjie Lei,[1] Fu B,[1] and Chaoshun Li[2]

SUMMARY

The integrated energy station of new energy vehicle hydrogenation/charging/power exchange is proposed, which also includes hydrogen production, hydrogen storage, electricity sales to users and the grid (WPIES). To address the efficiency of renewable energy use, this paper proposes a future value competition strategy for wind and photovoltaic (PV) allocation based on goal optimization (FVCS). In order to better realize the distribution of wind power/PV in the integrated energy station and improve the energy utilization efficiency of the integrated energy station, a two-layer optimization model of FVCS-WPIES is proposed, in which the upper layer model aims to maximize the expected income. The goals of the lower-level model are to maximize total profit, minimize battery losses, and minimize pollutant emissions. The model also considers the hydrogen power constraint and the upper-level model penalty. The comparison results show that the Pareto solution set is superior to the traditional model.

INTRODUCTION

With the increasing concern for environmental protection and energy security, how to improve energy efficiency and reduce pollution emissions has become the focus of global attention. In this background, the rapid increase in electric vehicle (EV) ownership and the change in energy supply structure have led the traditional gas station convert to an energy site that integrates renewable energy technologies. At the same time, wind and photovoltaic (PV) power generation widely applied in integrated energy station system design. The reason is that wind and PV and energy storage complementary technology can further improve operational efficiency and effectiveness of the integrated energy stations. Therefore, optimization methodology is the key to resolve these problems related to integrated energy station optimal scheduling and the wind and PV allocation in this research field.

Optimal scheduling of energy systems for integrated energy stations with EVs, Yuanzheng Li[1] developed a multi-objective optimization scheduling-based model for EV battery swapping stations (BSS) to minimize total operating costs while smoothing load fluctuations. Mingfei Ban[2] proposes a battery charging/swapping system based on wind power generation (W-BSCS), where wind turbines generate power to the grid while also participating in a centralized charging station (CCS), which can charge EV batteries centrally and then distribute fully charged batteries to multiple BSS, so the system also takes into account the vehicle routing problem (VRP). Hongtao Yuan[3] proposes a model for optimal operation in EV charging and storage, and establishes a battery fast charging model based on queuing theory, which can smooth the total load curve of the grid and finally achieve the effect of alleviating the peak-to-valley difference of the grid and reducing the total operating cost. Yuechuan Tao[4] proposes a data-driven two-stage charging and switching service scheme based on which users can independently select multiple service types. Finally, a joint deep reinforcement learning and mixed integer linear programming solution algorithm is proposed and used to solve the model. G.K. Zaher[5] proposed an EV charging and swapping model to determine optimal charging and discharging of EVs to maximize the profit of battery charging stations (BCS) owners, considering electricity price changes, grid connection limitations and battery capacity losses. Yang Wang[6] proposed two shadow price-based coordination methods, namely peer-to-peer method and leader-follower method based on EV charging stations, and established a two-layer optimization model to simulate the game between two non-cooperative entities, which solved by an improved nested column and constraint generation algorithm, which reduces the total operating cost by 10%. Most of the traditional EV charging and switching stations are planning models,[7–11] while the actual operation conditions of integrated energy stations are very complex. The aforementioned studies often consider one-sided factors only, and the models contain only single objective in these optimization problems, which cannot provide better decision-making solutions in the optimal scheduling of integrated energy stations. In order to solve the problem, Baojun Sun and Ridoy Das[12,13] proposed the concept of multi-objective techno-economic environment optimization for EV charging and discharging dispatching. Authors considered multiple objectives of battery degradation, grid interaction, CO_2 emission and user cost in the dispatching model. However, the former study does not consider the influence of

[1]Hubei Key Laboratory for High-efficiency Utilization of Solar Energy and Operation Control of Energy Storage System, Hubei University of Technology, Wuhan 430068, China
[2]Huazhong University Sci & Technol, Coll Hydroelect Digitizat Engn, Huazhong University of Science & Technology, Wuhan 430074, China
[3]Lead contact
*Correspondence: ma.jun@hbut.edu.cn
https://doi.org/10.1016/j.isci.2024.109305

battery cycle life, which is not conducive to the long-term operation of battery charging and swapping stations; the latter does not consider inclusion of clean energy sources such as wind and PV power generation. Alper[14] proposed an all-in-one EV station (AiOEVS) and solved the model through mixed integer linear programming, but the model did not consider wind power generation and electricity sales to the grid module. Mohd Bilal[15] introduced the Levy flight allocation strategy, adopted the improved salp swarm algorithm to optimize the scale of solar panels (SP) and wind turbines (WT) of the grid, and considered the probability of insufficient power supply. Mehdi Ahmadi[16] optimized the integrated microgrid energy management of battery charging and switching stations in the case of high energy critical loads and analyzed the risk of uncertainty using the conditional value-at-risk (VAR) index. In this paper, we combine the concept of many-objective optimization of the economic environment and the inclusion of clean energy sources such as wind power and PV to optimize the scheduling of the energy system of the integrated energy station.

For the objective-based optimization of duct power allocation problem, Zou Jianxiao[17] proposes a solar active power allocation method based on a multi-objective optimization technique, which simulates the active power allocation of the landscape by minimizing the error between the output power of the wind-photo-cell hybrid system and the desired power of the grid, minimizing the number of start/stop switches of the generation unit and maximizing the regulation capability of the wind turbine. Most active power control methods use batteries as filters to compensate the active power output and determine the control role based on different objectives.[18–20] The traditional active power distribution method tends to be more conservative in order to maintain the reliability and safety of the distribution network, based on the output power and rated power of the landscape power module for average distribution. In this paper, we combine the energy system dispatching of integrated energy station with the target-based wind and PV allocation strategy, which can further improve the model's optimal scheduling capability.

In order to better optimize the scheduling of the energy system model of the integrated energy station, this study proposes an optimal scheduling model of the integrated energy station with wind and PV based on the future value competition strategy (FVCS). The model optimizes the allocation of wind and PV by FVCS and solves the allocated wind-photovoltaic integrated energy station (WPIES) by adaptive non-dominated sorting genetic algorithm III[21] (ANSGA-III for short). Then, the entropy weight method (EWM) is applied to choose the final solution from the Pareto solution set for the decision making. Finally, a typical solution is analyzed to verify the reasonableness and reliability of the model. The main contributions of this paper are summarized as follows.

(1) Propose an FVCS based on an objective-optimized wind and PV power allocation method to improve the efficiency and reliability of energy system usage.
(2) The optimal scheduling model of wind power PV integrated energy station is proposed, which includes wind/PV/hydrogen production/hydrogen storage/high voltage charge/EV charge/EV swap/power grid modules. This model can better describe the energy management system of integrated energy station.
(3) Propose an FVCS-WPIES bi-level optimization model to improve multiple benefits, including economic and environmental, through an optimization-correction-optimization approach.

The components of this study are summarized as follows. Describes the optimal scheduling problem of the energy system of the integrated energy station and the FVCS-WPIES bi-level optimization model. Section 3 describes the proposed ANSGA-III algorithm which used to solve the FVCS-WPIES model. The model is compared to the literatures separately to verify the advantages of the FVCS-WPIES proposed in this study. Then, the final solution is chosen from obtained Pareto solution set according to the EWM. The typical solutions have been analyzed in the results. The results verify the rationality and reliability of the proposed model. Finally, the application prospect of FVCS-WPIES model has been discussed in detail. Schematic diagram of integrated energy station is shown in Figure 1. Finally, the fourth section makes a summary.

Problem statement and system model

This section introduces the models for each sub-module in FVCS-WPIES. It includes the wind turbine module, PV module, hydrogen production module, battery energy storage system (referred to as BESS) module (BCS and BSS), FVCS (the upper-level model), WPIES (the lower-level model), and the model constraints of FVCS-WPIES. Additionally, EVs contribute to charging and power exchange modules, while hydrogen vehicles contribute to hydrogen refueling modules.

Before optimizing and building the model, we make the following assumptions. (1) The compressor and hydrogen storage tank (HT) operate without hydrogen loss, and we calculate the capacity change of HT as equivalent to the state of charge (SOC) of BESS. (2) The SOC of each high voltage unit arriving at the integrated energy station follows a uniform distribution. (3) Let the number of batteries in the fully charged state be N_t^{full}, and the batteries in BCS and BSS are fully charged in 1 h. (4) The power prediction of the wind and PV power generation system of the integrated energy station is accurate enough and the output power fluctuation is stable. The wind and PV in this paper is simulated with constant values. (5) Each wind turbine and PV module can track the active power output.

Figure 2 displays the microgrid access schematic of the grid-connected FVCS-WPIES model. The power generated by wind and PV can be supplied to the battery swapping stations (BSS), BCS, electrolyzer, and compressor. The electrolyzer utilizes the supplied power to generate hydrogen, while the compressor compresses the hydrogen generated by the electrolyzer. The compressed hydrogen is stored in the HT, which can then be used to purchase additional power from the grid. This is particularly useful when wind power alone cannot meet the load demand of each sub-module. The solid black line in the figure represents the power flow, while the red dashed line represents the hydrogen flow.

Many scholars have made contributions in the field of integrated energy station optimization scheduling. Optimizing the schedule for an integrated energy station involves multiple objective functions and modules for PV, wind energy, and EV charging/swapping. To demonstrate

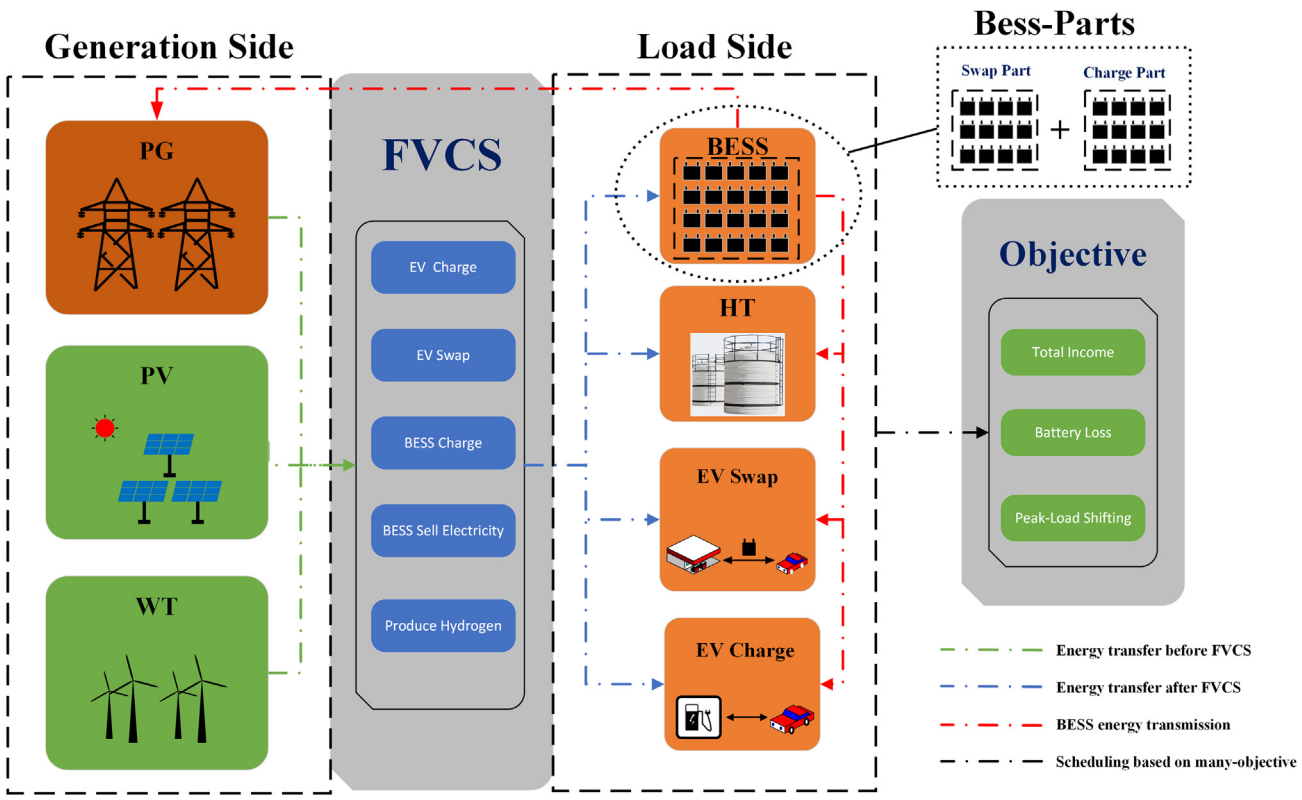

Figure 1. Schematic diagram of FVCS-WPIES model

the benefits and versatility of the FVCS-WPIES model, this paper compares it with the existing integrated energy station optimization scheduling model. The specific comparison details are presented in Table 1.

The proposed WPIES model, as shown in Table 1, includes more modules and better reflects the operating conditions of integrated filling stations compared to existing research studies on optimal scheduling. To improve the solution method, an improved NSGA-III algorithm is used along with the FVCS scheduling strategy in this paper. This combination results in a more efficient solution for the model.

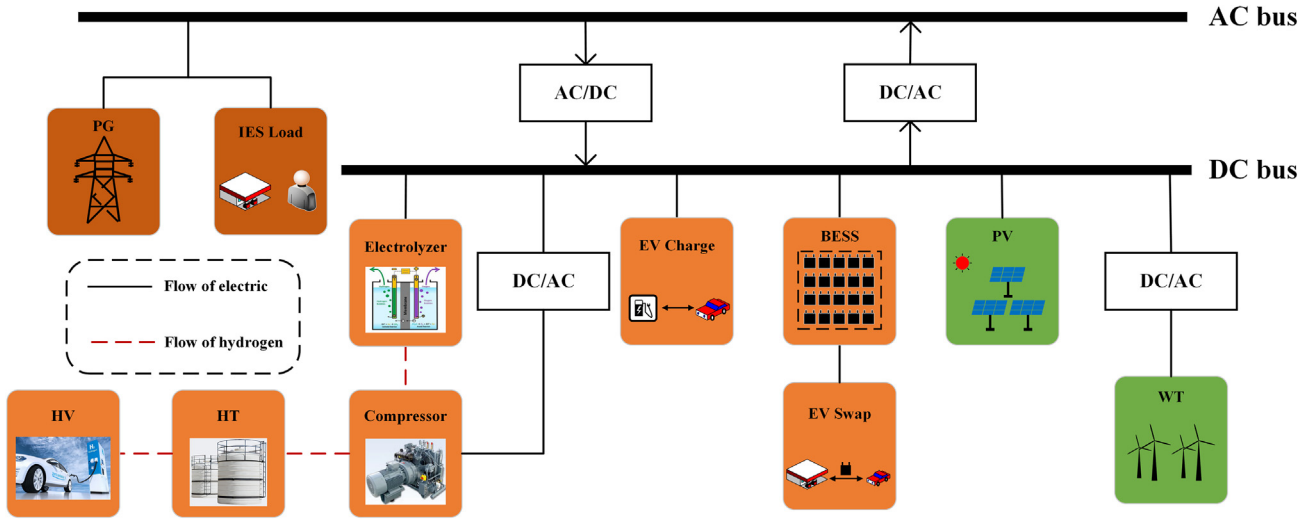

Figure 2. Schematic diagram of grid-connected FVCS-WPIES microgrid access

Table 1. The model comparison difference of existing research results

Reference	Components								Objectives	Method
	EV charge	EV swap	HVs	PV	Wind	Grid	BESS	Hydrogen		
Sun et al.[13]	✓	×	×	✓	✓	✓	✓	×	Cost Pollution emissions	MOPSO TOPSIS
Das et al.[12]	✓	×	×	×	×	✓	✓	×	Energy cost Battery degradation Grid net exchange CO_2 emission	MOO MCDM
Zaher et al.[5]	✓	✓	×	×	×	✓	✓	×	BES profit	MIP
Li et al.[1]	✓	✓	×	✓	×	✓	✓	×	Inventory Cost Smoothing load fluctuation	Modified NSGA-III
Saner et al.[22]	✓	×	×	×	×	✓	×	×	Demand Energy charges	Linear Programming
Su et al.[23]	✓	×	×	×	×	✓	×	×	Load recovery Power distribution network economy EV driving cost	Piecewise Linearization SOCR
Wu et al.[24]	✓	×	×	×	×	✓	×	×	Charging cost	Linear Programming
Dai et al.[25]	✓	×	×	✓	×	✓	✓	×	Total cost	MAPSO
Zhang et al.[26]	✓	×	×	×	✓	✓	×	×	Cost of generating electricity Wind curtailment rate	Two-phase strategy IMOEA
Hao et al.[27]	✓	×	×	✓	×	✓	×	×	Total revenue	Stackelberg GA
Shojaabadi et al.[28]	✓	×	×	×	✓	✓	×	×	Total revenue	A Game Theory
Dukpa et al.[29]	✓	×	×	×	✓	✓	×	×	Total revenue	Linear Programming
Amiri et al.[30]	✓	×	×	×	×	✓	×	×	Charging cost Busbar voltage deviation	NSGA-II
Shi et al.[31]	✓	×	×	✓	×	✓	×	×	Total cost	Robust Optimization Algorithm
Wen et al.[32]	✓	×	×	✓	×	✓	✓	×	Total cost	DRNN-LSTM PSO
Xu et al.[33]	×	✓	✓	×	✓	✓	✓	✓	Total operational cost	Hybrid Stochastic/Distributionally Robust Optimization
Ours	✓	✓	✓	✓	✓	✓	✓	✓	Total profit Battery loss Pollutant Emissions	Future Value Competition ANSGA-III

Wind turbine model

Wind speed and tower height directly affect the power produced by wind turbines. The article uses the wind turbine model proposed byXu et al.[34] to estimate the power generation of wind turbines in integrated energy addition stations:

$$P_{WT} = \begin{cases} 0 \\ \dfrac{P_R}{V_R^3 - V_{ci}^3} \cdot V^3 - \dfrac{V_{ci}^3}{V_R^3 - V_{ci}^3} \cdot P_R \\ P_R \\ 0 \end{cases} \quad \text{(Equation 1)}$$

where V, P_R, V_R, V_{ci} and V_{co} are the actual wind speed at the hub height of the wind turbine (m/s), the rated power of the wind turbine (kW), the rated wind speed (m/s) and the cut-in and cut-out wind speeds (m/s), respectively.

Table 2. Photovoltaic panel parameters

	η_{inv}	η_{loss}	η_{ref}	k
Value	0.95	0.86	0.12	0.004

Photovoltaic model

The power generation of PV is determined by several parameters, the solar load on the surface of the PV panel (G_β) in W/m², the working temperature of the PV panel (T_0) in °C, the inverter efficiency (η_{inv}) and the loss (η_{loss}) in %, the power generation of the PV module can be expressed as[35]:

$$P_{PV} = [\eta_{inv} \cdot \eta_{loss} \cdot \eta_{ref} \cdot (1 - k \cdot (T_0 - T_{ref}))] \cdot A_{PV} \cdot G_\beta \quad \text{(Equation 2)}$$

where η_{ref} is the benchmark efficiency of PV module at the benchmark temperature of 25°C (T_{ref}), unit is %. k is the temperature coefficient. A_{PV} is the planned area of the PV array in the hybrid system (m²). Most of the data in the formula are provided by the manufacturer, as shown in Table 2.

Hydrogen production system model

Electrolyzer model. Hydrogen gas is produced through the process of electrolysis of water. The overall reaction can be represented by Equation 3. One of the most beneficial factors of using a polymer electrolyte membrane (PEM) electrolyzer is that it operates at a low temperature and has a simple structure. The high purity hydrogen gas can be produced when the pressure goes up to 200 bar.[33] The calculation model of electrolytic water conversion for PEM electrolyzer is shown in Equation 4.[36]

$$H_2O + Electricity \rightarrow H_2 + \frac{1}{2}O_2 \quad \text{(Equation 3)}$$

$$P_t^{ELE} = \frac{m_t^{ELE} \cdot LHV_{H_2}}{\eta_{ELE}} \quad \text{(Equation 4)}$$

where η_{ELE} is the electrolyzer efficiency. m_t^{ELE} is the mass flow rate of hydrogen gas at the output of the electrolyzer. LHV_{H_2} is the lower calorific value of hydrogen. P_t^{ELE} is the power consumed by the electrolyzer at time t. The specific parameter values in the electrolyzer are shown in Table 3.

Compressor model. The compressor works alongside the process of electrolyzing water to produce hydrogen. It is powered by a combination of the PV module, the WT module, and the power grid. The compressor's job is to increase the pressure of the hydrogen from the low-pressure storage tank to the high-pressure storage tank. Equation 5 shows the model of the compressor. In this paper, we assume that there is no hydrogen loss during the compression process.[37]

$$P_t^{comp} = C_{comp} \cdot \frac{T_{in} \times 10^4}{\eta_{motor} \cdot \eta_{comp} \cdot \Delta t} \left(\left(\frac{p_{out}^{comp}}{p_{in}^{comp}} \right)^{\frac{r-1}{r}} - 1 \right) \cdot \frac{m_t^{ELE}}{3600} \quad \text{(Equation 5)}$$

where C_{comp} denotes the specific heat of hydrogen at constant pressure. P_t^{comp} denotes the power consumed by the compressor motor at time t. p_{in}^{comp} and p_{out}^{comp} are the compressor inlet pressure and outlet pressure, respectively. r denotes the specific heat ratio of hydrogen. T_{in} indicates the hydrogen temperature at the compressor inlet. η_{comp} is the isentropic efficiency of the compressor. η_{motor} is mechanical efficiency. The specific parameter values in the compressor are shown in Table 4.

Hydrogen storage tank model. The purpose of the HT is to store hydrogen that is compressed and then supplied to the distributor as needed to meet hydrogen demand for the HVs. This paper transforms the variation of hydrogen content in the HT into the form of electricity variation in BESS. Equation 6 shows the variation of hydrogen content in the HT.

$$SOC_{t+1}^{HT} = \left[(1 - \varphi^{HT}) \cdot SOC_t^{HT} + (m_t^{ELE} - m_t^{HV}) \cdot C_{HT} \right] \quad \text{(Equation 6)}$$

where SOC_t^{HT} and SOC_{t+1}^{HT} are the hydrogen storage content in HT at time t and t+1, respectively, unit is %. m_t^{HV} is the hydrogen supplied to HVs at time t. φ^{HT} is the coefficient of hydrogen loss that occurs in HT. C_{HT} is the total capacity of HT. The specific parameter values in the HT are shown in Table 5.

Table 3. Electrolyzer parameters

	η_{ELE}	LHV_{H_2}
Value	62%	33.3 kWh/kg

Table 4. Compressor parameters

	C_{comp}	T_{in}	η_{comp}	p_{in}^{comp}	p_{out}^{comp}
Value	14.304 kJ/kg	293K	70%	1MPa	90MPa

Vehicle flow modeling under TOU

Analyze and record statistics on the travel characteristics of electric cabs, electric private cars and hydrogen vehicles in a month, and simulate the initial SOC state of car users when they arrive at the integrated energy station. Combined with the EVs charging and swapping expectations, the resulting data are in line with the normal distribution.[13] The SOC for EVs and hybrid vehicles (HVs) are uniformly distributed upon arrival at the integrated energy station. U_{HV} : (0.2 , 0.5). Integrated energy stations can offer charging and swapping services for EVs. When an EV arrives at the station, the SOC will determine whether charging or swapping is required. The station will select the appropriate service based on the time required for each mode of charging. When the battery level (SOC) of an EV is less than 20%, users may consider fast charging due to the increased time cost. However, fast charging can cause excessive battery loss. In such situations, users prefer battery swapping service. To facilitate this, the integrated energy station sets the initial SOC to less than 20% when the EV arrives, allowing the refueling station to classify it as a power exchange mode. If the initial SOC is greater than 20%, it is classified as a charging mode. The simulated hourly charging load of EVs, power exchange load, and hourly hydrogen demand of hydrogen vehicles are shown in Figure 3. In this paper, the hydrogen demand of hydrogen vehicles is converted to electrical load demand for comparison. The simulated power generation of PV and wind power in this region is shown in Figure 4.

In the optimal scheduling of integrated energy systems, demand side management (DSM) can reduce total operating costs and separate elastic and inelastic loads.[38–40] Therefore, this paper has used the local time-of-use (TOU) price as the price for WPIES to buy electricity from the grid, and the purchase price of user EVs and the price of selling to the grid have also changed with the change of TOU price. The TOU is shown in Figure 5.

BESS model

For the swapping mode, the BESS model requires the battery SOC to be charged to 90% before it can be used for EVs swapping. For charging mode, BESS uses the charger to charge the battery and discharges the EVs and the regional power system at the same time. With the premise that charging and discharging states cannot be performed simultaneously, battery SOC states in the 90%–20% interval are possible. In the optimization model developed in this study, two types of services are provided for EVs: charging and swapping. Combined with the aforementioned analysis, the model is undoubtedly very difficult and complex if the charging and swapping models are analyzed in a unified way in the BESS module. Therefore, in order to simplify the model, the BESS module is split into a BCS and a BSS, and the two modules are modeled separately and calculated uniformly. This has several advantages. (1) When the EV changes the undercharged battery at the BSS, the BSS charges the undercharged battery during that time period, while the BSS charges and discharges in the context of considering the time-sharing tariff. (2) EVs are charging and swapping at the same time, while the total revenue of the integrated charging station is only calculated for the total discharge of the BESS, the charging/swapping demand and the purchased power from the grid. (3) When in high tariff time, the batteries in the BCS module are in charging state, and the spare fully charged batteries in the BSS module can be discharged after meeting the EV swapping demand, thus reducing the total power purchased by the BESS from the grid. The structure of the BESS model is shown in Figure 6.

BCS model in BESS. In the charging mode of BESS, the charging and discharging process of the battery is shown in Equation 7.

$$SOC_t^{BCS} = \frac{\left[E_{t-1}^{BCS} \times (1 - \sigma) + P_{charge,t} \times \eta_{charge} \times \Delta t_1 - P_{disharge,t} \times \eta_{disharge} \times \Delta t_2\right]}{C_{BCS}} \quad \text{(Equation 7)}$$

where SOC_t^{BCS} is the SOC state of BCS at time t. E_{t-1}^{BCS} is the charge of BCS at time t-1. σ is the self-discharge rate of the battery. $P_{charge,t}$ is the charging power of the battery at time t. η_{charge} is the charging efficiency of battery. $P_{disharge,t}$ is the discharge power of the cell at time t. $\eta_{disharge}$ is the discharge power of battery. Δt_1 and Δt_2 are the charge interval and discharge interval of the battery, respectively. C_{BCS} is the total battery capacity of BCS.

BSS model in BESS. There are two states that the battery can be in: charged and fully charged in BESS's swapping mode. When a car arrives, the fully charged battery is swapped with the EV and the swapped battery is charged using the charger. It is assumed that each battery

Table 5. Parameters of hydrogen storage tank

	φ^{HT}	C_{HT}
Value	0.01%	60kg

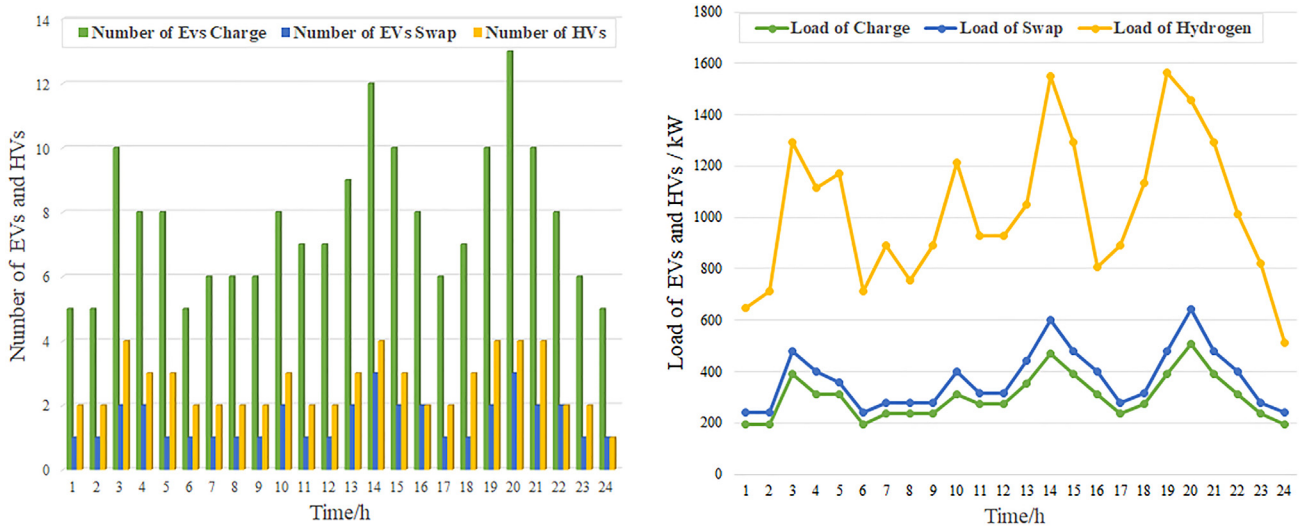

Figure 3. Number of EVs and HVs and power load

needs to be fully charged within 1 h. The number of fully charged cells is N_t^{full}. The number of batteries in charge state is N_t^{charge}. The dynamic model of the battery swapping station is represented as follows.

$$\begin{cases} N_t^{full} = N_{t-1}^{full} - N_{t-1}^{EV,BSS} \\ W_t^{BSS} = \sum_n^N \left[\left(0.9 - SOC_{t-1,n}^{EV,BSS} \right) \times C_{Battery} \right] \end{cases} \quad \text{(Equation 8)}$$

where A is the number of fully charged cells at t-1. $N_{t-1}^{EV,BSS}$ is the number of EVs exchanged for electricity at t-1. W_t^{BSS} is the amount of electricity consumed by the battery after the swapping station and the EVs are fully charged in time t. $SOC_{t-1,n}^{EV,BSS}$ is the SOC state of the battery at the time of arrival of the n-th electric car swapping at t-1. $C_{Battery}$ is the capacity of a single battery. In order to be able to meet the demand of the next time period for the EV swapping, at time t the BSS will charge the battery swapped out before time t-1 to a full charge.

Upper-level model

This paper discusses the challenges of integrating wind and PV power generation with TOU rates, EV and HV consumption. These uncertainties can cause varying degrees of wind and PV abandonment in the integrated energy station, which in turn reduces the station's total revenue. To address this issue, the paper proposes a bi-level optimal scheduling model based on the FVCS. By separating wind and PV power

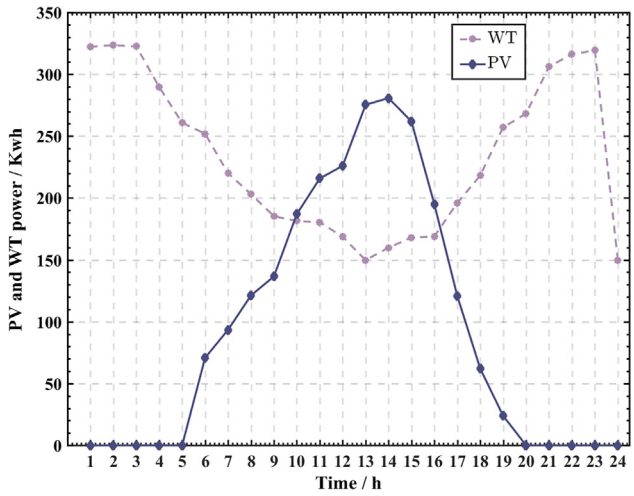

Figure 4. PV and WT power generation

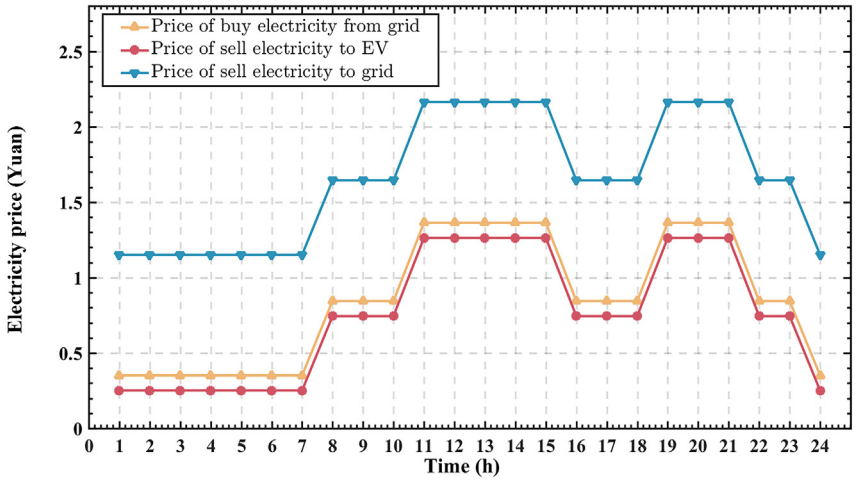

Figure 5. Charging and discharging price of integrated energy station

in the integrated energy station, the upper-level model is constructed. The optimal allocation scheme of wind and PV power is then deduced through the FVCS.

Future value competition strategy. In the upper-level model, PV and wind power are allocated to the EV charging module, hydrogen production module, and Bss module respectively through a FVCS. Under the background of TOU, the operation and control conditions of the energy system of the integrated energy station will change with the different power of PV and wind power generation at different times, and the benefits generated will be different. Therefore, the FVCS proposed in this paper changes the previous wind and PV system power distribution in an average way. The allocation of the active power of the wind and PV in the integrated energy station is controlled by the wind and PV energy allocation strategy based on target optimization, thus changing the energy share of each subsystem in the integrated energy station. In the optimization process of the lower-level model (WPIES), the distribution value of wind/PV of each module is random, which affects the electricity purchased by each module from the grid at each moment, and finally affects the overall income of the integrated energy station. The upper-level model (FVCS) was used for pre-distribution to solve the power allocation scheme with the maximum total return. After solving the WPIES model, the return objective function was compared with FVCS in order to enhance the active power distribution value of wind/PV and improve the optimization outcome of the FVCS-WPIES model. The principle of FVCS is illustrated in Figure 7.

FVCS calculates the distribution of active power from the wind and PV system to each subsystem by measuring the expected benefit of the energy generated by the wind and PV flowing into each subsystem of the integrated energy station and solves the optimization model using the Harris Hawks algorithm (HHO).[41]

To enhance the accuracy of the upper-level model, penalty functions are added to it. Once the lower-level model is resolved, if the actual operating conditions during time period t fail to achieve the anticipated profit, the objective function value of the upper-level model is penalized. The penalty function can be expressed in the following manner.

$$\sum_{i=1}^{m} \omega_i \max\{0, x_1 - x_2\} \quad \text{(Equation 9)}$$

where ω_i denotes the penalty weight. x_1 denotes the value of the optimized objective function, i.e., the expected profit. x_2 denotes the actual profit after optimization of the lower-level model.

Upper-level model objective function. The objective function of the upper-level model is to maximize the expected profit. Electricity allocated to the hydrogen production module is converted into hydrogen for HV hydrogenation, and the electricity allocated to the BESS module is sold to the grid. The expected profit objective function of the upper-level model is shown in Equation 10.

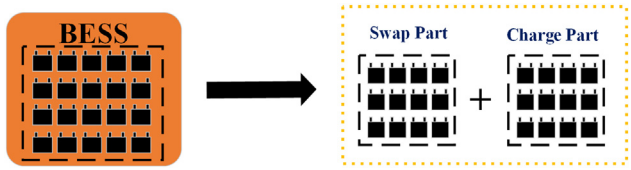

Figure 6. Schematic diagram of BESS model

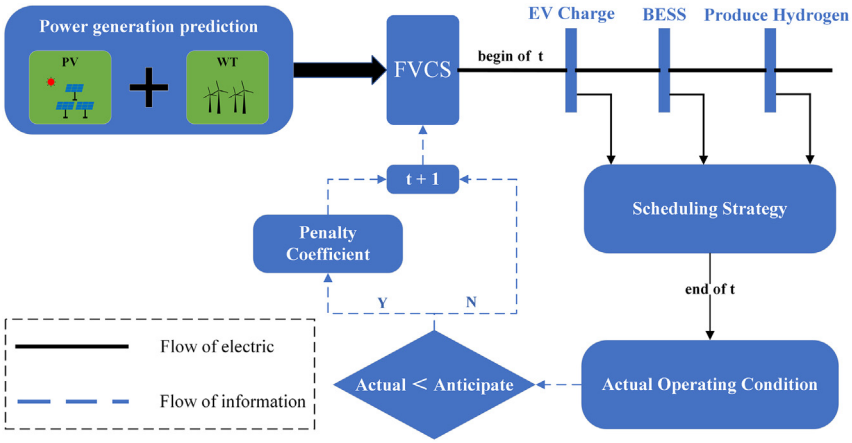

Figure 7. FVCS schematic

$$\max F_{profit}^{FVCS} = \sum_{t=1}^{T} W_t^{BESS,WP} \times P_{discharge,t}^{price} + W_t^{EV,WP} \times P_{sell,t}^{price} + W_t^{HT,WP} \times \eta_{H_2} \times P_{H_2}^{price} \quad \text{(Equation 10)}$$

where $W_t^{BESS,WP}$ is the amount of power allocated to BESS through FVCS in time period t. $P_{discharge,t}^{price}$ is the price of electricity sold to the grid in time period t. $W_t^{EV,WP}$ is the amount of power allocated to the EV charging module via FVCS in time period t. $P_{sell,t}^{price}$ is the price of EV charging at time t. $W_t^{HT,WP}$ is the amount of power allocated to the hydrogen production module through FVCS in time t. $P_{H_2}^{price}$ is the price of selling hydrogen. η_{H_2} is the efficiency of converting electricity to hydrogen.

Lower-level models

This section presents the economic, operational and environmental objectives pursued for the optimal operation of integrated energy stations. At the core of the lower-level model energy management are three objective functions, consisting of maximizing total revenue, minimizing battery losses and minimizing pollutant emissions, respectively.

Maximum total profit. From the perspective of the operation of an integrated energy station, the total profit of a station is a fundamental goal. Energy management of EVs, hydrogen vehicles and the power grid based on TOU can maximize the operational benefits of integrated energy stations. In this study, the total profit objective function of the integrated energizing station is shown as flows. The algorithm in the code solves for the minimum value of the objective function. Therefore, we take the negative of the total profit objective function in the code to obtain the minimum value as the result.

$$\max F_{profit}^{WPIES} = f_{profit}^{BCS} + f_{profit}^{BSS} + f_{profit}^{EV} + f_{profit}^{HT} \quad \text{(Equation 11)}$$

$$W_t^{BESS,WP} = W_t^{BCS,WP} + W_t^{BSS,WP} \quad \text{(Equation 12)}$$

$$\begin{cases} f_{profit}^{BCS} = \sum_{t=1}^{T} P_{discharge,t}^{BCS} \times \Delta t_2 \times P_{discharge,t}^{price} - \left(P_{charge,t}^{BCS} \times \Delta t_1 - W_t^{BCS,WP} \right) \times P_{buy,t}^{price} \\ f_{profit}^{BSS} = \sum_{t=1}^{T} \left[0.9 C_{Battery} \times N_t^{EV,BSS} \times P_{sell,t}^{price} - \left(W_t^{BSS} - W_t^{BSS,WP} \right) \times P_{buy,t}^{price} \right] \\ f_{profit}^{EV} = \sum_{t=1}^{T} P_{charge,t}^{EV} \times \Delta t_2 \times P_{sell,t}^{price} - W_{charge,t}^{EV} \times P_{buy,t}^{price} \\ f_{profit}^{HT} = \sum_{t=1}^{T} Q_t^{HV} \times P_{H_2}^{price} - \left(\frac{\Delta SOC_{t,t-1}^{HT} \times C_{HT}}{\eta_{H_2}} - W_t^{HT,WP} \right) \times P_{buy,t}^{price} \end{cases} \quad \text{(Equation 13)}$$

where $P_{discharge,t}^{BCS}$ and $P_{charge,t}^{BCS}$ are divided into the discharging power and charging power of BCS at time t. $P_{buy,t}^{price}$ is divided into the price of electricity purchased from the grid in time t. $P_{charge,t}^{EV}$ is the charging power of EV at time t. $W_{charge,t}^{EV}$ is the amount of electricity purchased from the grid by the EV charging module at time t. Q_t^{HV} is the weight of hydrogen required for HVs in time period t. $\Delta SOC_{t,t-1}^{HT}$ is the change in hydrogen SOC of HT in time t and time t-1.

Table 6. Pollutant emission data by power generation type

Power generation methods	SO_2 (g)	NO_x (g)	CO_2 (g)
Photovoltaic power	0	0	20
Wind power	0	0	11
Nuclear power	0	0	12
Coal-fired power	26	13	872
Gas-fired power	2	50	400
Oil power	20	30	800
Utility grid	30	15	997

Minimal battery loss. Reducing the Bss of integrated energy station can effectively increase the operating life of integrated energy station. The main factors of battery wear are related to the number of cycles, operating temperature, charging and discharging efficiency, depth of discharge (DOD), SOC, and end-of-charge voltage (EOCV).[42] Therefore, in the WPIES model, the wear factor (kW·h/kW·h) for Li-ion batteries with the same achievable cycle count depth of discharge (ACC-DOD) characteristics. This value is mainly related to the change in total battery energy. Ignoring other factors in this application. In this study, the minimum objective function of the loss of the BESS in the integrated energy station is shown as follows.

$$\min F_{loss}^{WPIES} = K_w \sum_{t=1}^{T} P_{charge,t}^{BCS} \times \Delta t_1 + P_{discharge,t}^{BCS} \times \Delta t_2 + W_t^{BSS} \quad \text{(Equation 14)}$$

where $K_w = 0.00015\text{kW}\bullet\text{h}$. This means that each kW·h of charging or discharging of the EV battery will reduce the available energy of the Li-ion battery by approximately 0.00015 kW h.

Minimal pollutant emissions. Pollutants in conventional thermal power plants are mainly composed of SO_2, NO_x, CO_2, CO and suspended particulate matter (TSP). The development and utilization of WPIES can effectively reduce the emission of the aforementioned pollution, thus reducing environmental pollution. Specific emission data for wind, PV, nuclear, coal-fired, gas-fired, and oil-fired power generation are shown in Table 6.

Application of the WPIES model will positively reduce global carbon emissions. The load of the integrated energy station is mainly provided by wind power and PV power generation. In this study, the environmental pollution emissions from the integrated energy station are mainly caused by the electricity purchased from the grid. Therefore, the objective function is to minimize the emissions of SO_2, NO_x and CO_2. The objective function is as follows.

$$\min F_{CO_2,SO_2,NO_x}^{WPIES} = \sum_{t=1}^{T} W_{buy,t}^{Grid} \times \left(e_{CO_2} + e_{SO_2} + e_{NO_x}\right) \quad \text{(Equation 15)}$$

$$W_{buy,t}^{Grid} = P_{charge,t}^{BCS} \times \Delta t_1 + W_t^{BSS} + W_{charge,t}^{EV} + \frac{\Delta SOC_{t,t-1}^{HT} \times C_{HT}}{\eta_{H_2}} - W_t^{WP} \quad \text{(Equation 16)}$$

where $W_{buy,t}^{Grid}$ is the amount of electricity purchased from the grid by WPIES in time period t. e_{CO_2}, e_{SO_2} and e_{NO_x} are the emission factors of SO_2, NO_x and CO_2 per kW·h from the utility grid, respectively. W_t^{WP} is the amount of wind and PV power generated at time t.

Model constraints

Hydrogen power constraint

Hydrogen electrolysis requires a large amount of electricity, and the hydrogen obtained by electrolysis of water needs to go through a compressor and then to a HT, and the whole process takes some time. When HVs require more hydrogen than can be supplied by wind and PV outputs, and the Bss cannot meet the demand, a hydrogen balance equation can be used to fully meet the requirement. However, in such a scenario, a large amount of electricity is needed for hydrogen electrolysis, which has to be purchased from the grid. This can significantly increase the power purchase cost of the integrated energy station. Therefore, this paper introduces a chance-constrained hydrogen equilibrium equation. Valuation confidence level based on the risk appetite of the decision maker[33,43] to allow for integrated energy stations that do not need to purchase large amounts of power from the grid when electricity prices are high and wind/PV output is insufficient. This will result in hydrogen demand for HVs that may not always be met.

$$P_r = \left\{m_t^{HV} \geq \xi_t\right\} \geq 1 - \alpha \quad \text{(Equation 17)}$$

where A is the hydrogen demand of HVs. α is a predefined small probability index.

Other constraints

The energy control in FVCS-WPIES formulates the optimal operation strategy of the system based on the charging/discharging load of the EV battery, the battery scheduling of the EV power swapping module, and the hydrogen production rate of the hydrogen production system to achieve the power balance of the whole system. The following constraints also need to be satisfied in the optimal scheduling of integrated energy stations.

Capacity constraint. The constraint is for the Bss and hydrogen storage system of the integrated energy station, the energy storage system cannot be higher than the maximum capacity of the system and cannot be smaller than the minimum capacity of the system. In this study, the capacity state of the HT is transformed into the load state of the EV battery. The formula is shown as follows.

$$SOC_{\min}^{HT} \leq SOC_{t}^{HT} \leq SOC_{\max}^{HT} \quad \text{(Equation 18)}$$

$$SOC_{\min}^{BESS} \leq SOC_{t}^{BESS} \leq SOC_{\max}^{BESS} \quad \text{(Equation 19)}$$

$$SOC_{\min}^{BESS} = (1 - DOD) \times SOC_{\max}^{BESS} \quad \text{(Equation 20)}$$

$$SOC_{\min}^{HT} = 0, SOC_{\max}^{HT} = 1, SOC_{\min}^{BESS} = 0.9, SOC_{\max}^{BESS} = 0.2 \quad \text{(Equation 21)}$$

where $SOC_{\min}^{HT}$ and $SOC_{\max}^{HT}$ are the minimum and maximum capacity states of the HT, respectively. $SOC_{\min}^{BESS}$ and $SOC_{\max}^{BESS}$ are the minimum load state and maximum load state of EV battery, respectively. DOD is the maximum DOD allowed for the battery. SOC_{t}^{BESS} is the load state of the BESS at time t. Too high or too low EV battery load state will cause rapid reduction of battery cycle life and energy storage efficiency, so from the perspective of long-term operation of integrated energy station, this study constrains the maximum and minimum values of EV load state, i.e., [0.2,0.9]. To ensure the energy supply of the Bss and the hydrogen storage system the next day, the load state of the batteries in the BCS module at the end of the day is the same as the load state at the beginning. The capacity state of the hydrogen storage system at the end of the day is the same as the capacity state at the beginning. The number of fully charged cells in the BSS module should remain the same at the end of the day as it was at the beginning.

$$SOC_{0}^{HT} = SOC_{T}^{HT} \quad \text{(Equation 22)}$$

$$SOC_{0}^{BCS} = SOC_{T}^{BCS} \quad \text{(Equation 23)}$$

$$N_{0}^{full} = N_{T}^{full} \quad \text{(Equation 24)}$$

where SOC_{0}^{HT}, SOC_{T}^{HT} are the capacity states of HT at the beginning and end of the day, respectively. SOC_{0}^{BCS}, SOC_{T}^{BCS} are the load states of the cells in the BCS at the beginning and end of the day, respectively. N_{0}^{full}, N_{T}^{full} are the number of fully charged cells in the BSS at the beginning and end of the day, respectively.

Power constraint. This constraint is for electrolyzer power and EV battery charge/discharge power. The battery in BESS cannot exceed the maximum discharge power and cannot be lower than the minimum discharge power. Electrolyzer cannot exceed the maximum power consumption and cannot be lower than the minimum power consumption. The constraint formula is shown as follows.

$$\begin{cases} 0 \leq P_{discharge,t}^{BESS} \leq P_{discharge,\max}^{BESS} \\ 0 \leq P_{charge,t}^{BESS} \leq P_{charge,\max}^{BESS} \end{cases} \quad \text{(Equation 25)}$$

$$P_{\min}^{ELE} \leq P_{t}^{ELE} \leq P_{\max}^{ELE} \quad \text{(Equation 26)}$$

where $P_{\min}^{ELE}$ and $P_{\max}^{ELE}$ are the minimum power consumption and maximum power consumption of the electrolyzer, respectively.

Energy balance constraint. The power balance problem in this constrained output model is a prerequisite for the stable operation of the FVCS-WPIES system. In this system, the daily energy generation and consumption should be equal, and the power allocated by the upper-model should be equal to the power added by the lower-level model.

$$P_{buy,t}^{Grid} = \left(P_{charge,t}^{BCS} + P_{charge,t}^{BSS} + P_{charge,t}^{HT}\right) \times \eta_{charge} + P_{charge,t}^{EV} - P_{t}^{WP} \quad \text{(Equation 27)}$$

$$P_{discharge,t}^{Grid} = \frac{P_{discharge,t}^{BCS} + P_{discharge,t}^{BSS}}{\eta_{discharge}} \quad \text{(Equation 28)}$$

$$W_{t}^{FVCS} = W_{t}^{WPIES,WP} \quad \text{(Equation 29)}$$

Table 7. Algorithm and model specific parameters

	N_p	T_{max}	C_r	m	m_{BCS}	m_{BSS}	C_{HV}	C_{HT}	$P_{H_2}^{price}$
Value	400	1000	60 kW h	20	15	5	6Kg	60Kg	58Yuan/Kg

where $P_{buy,t}^{Grid}$ is the power at time t when power is purchased from the grid. $P_{charge,t}^{HT}$ is the charging power of the hydrogen production system at time t. P_t^{WP} is the power supply of the wind and PV in time t. $P_{discharge,t}^{Grid}$ is the power sold to the grid in time t. W_t^{FVCS} is the power allocated to the WPIES system by the upper-model. $W_t^{WPIES,WP}$ is the power received by the WPIES system from the wind and PV system at time t.

Energy storage system state constraints. In BCS and BSS systems, a single EV battery is not allowed to be charged and discharged at the same time, but it is allowed to have a scenario where some batteries are in charging state while others are in discharging state. In hydrogen production systems, simultaneous charging and discharging is allowed. The constraint formula is shown as follows.

$$\ell_{\Delta t_1} + \ell_{\Delta t_2} = [0,1] \quad \text{(Equation 30)}$$

$$\ell_{\Delta t_1} = [0,1] \quad \text{(Equation 31)}$$

$$\ell_{\Delta t_2} = [0,1] \quad \text{(Equation 32)}$$

where $\ell_{\Delta t_1}$, $\ell_{\Delta t_2}$ are the charge state coefficient and discharge state coefficient, respectively. 1 means the battery is in charging or discharging state, 0 means it is not in charging or discharging state.

RESULTS

In this section, we will first solve the two models separately using the multi-objective algorithm ANSGA-III. After finding the optimal solution, we will compare the objective functions to verify the advantages of the FVCS-WPIES model. Next, we will use the entropy method to filter the Pareto solution set obtained from the optimal solution of the FVCS-WPIES model, and select the optimal decision solution. Finally, we will validate and analyze the selected optimal decision solution. The simulation experiments were conducted in MatlabR2021b with a computer configuration of CPU 3.20 GHz, RAM 16.0 GB. The specific parameters of the algorithm and the model are shown in Table 7.

Model comparison

In order to confirm the effectiveness of the FVCS-WPIES model presented in this paper, a comparison model was used. The comparison model employed the optimal scheduling model of the energy system of an integrated energy station, but without the FVCS strategy. This model only utilizes the WPIES model and follows the scenario of the average wind and PV power distribution in conventional vehicle charging stations. The ANSGA-III algorithm was improved on NSGA-III by introducing an adaptive parameter control strategy that can automatically adjust the parameter values according to the characteristics of the problem and improved several strategies in NSGA-III. The specific contents are as follows: (1) improve the elitist selection operator; and (2) improve the creation of offspring population, thus improving the algorithm performance. In this paper, we optimally solved the FVCS-WPIES model and the comparison model using the ANSGA-III algorithm. The Pareto front resulting from the solution is shown in Figure 7. The code of the improved part of the ANSGA algorithm is as follows.

Algorithm 1. Tournament selection (p_1, p_2) procedure

Require: p_1, p_2
Ensure: p'

1: if feasible(p_1) = TRUE and feasible(p_2) = FALSE then
2:$p' = p_1$
3: else if feasible(p_1) = FALSE and feasible(p_2) = TRUE
then
4: $p' = p_2$
5: else if feasible(p_1) = FALSE and feasible(p_2) = FALSE
then
6: if CV(p_1) > CV(p_2) then
7: $p' = p_2$
8: else if CV(p_1) < CV(p_2) then
9: $p' = p_1$
10: else
11: p' = random(p_1, p_2)
12: end if
13: else
14: p' = random(p_1, p_2)
15: end if

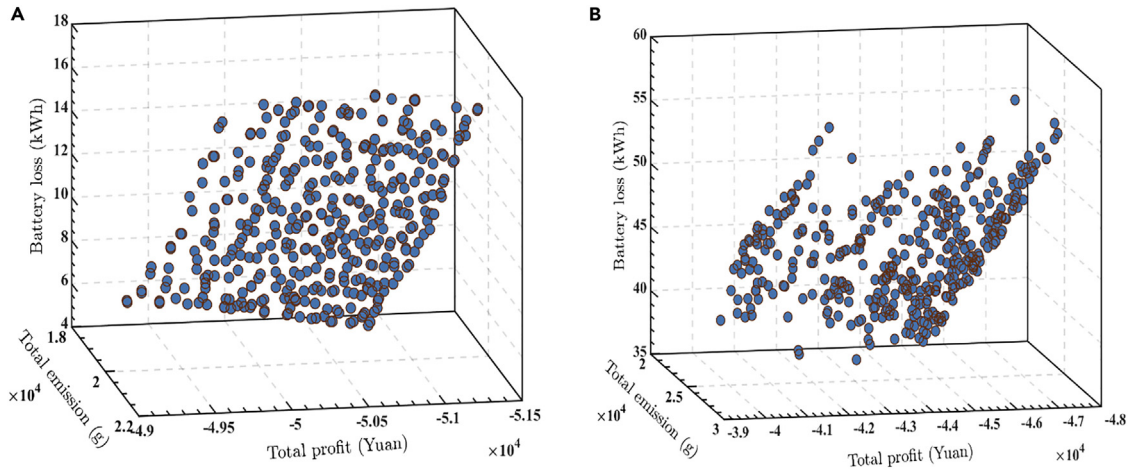

Figure 8. Pareto frontier of two models

(A) FVCS-WPIES model.

(B) Comparison model.

As can be seen from Figure 8, the Pareto front obtained by FVCS-WPIES model after adding FVCS strategy is more evenly distributed than the Pareto front of WPIES model, with better value of each objective function. Next, we will compare all the schemes of the three objective functions and analyze them.

From Figure 9, it can be seen that the three objective functions of the FVCS-WPIES model are smaller than the comparison model. The objective function F_{profit}^{WPIES} was reduced by 6389(Yuan) compared to the comparison model. That is, total profit is on average 12.67% higher than the comparison model. The objective function $F_{CO_2,SO_2,NO_x}^{WPIES}$ was reduced by 5,446.64 (g) compared to the comparison model. On average, the total emissions are 21.65% lower than the emissions produced by the comparison model. The objective function is reduced by 34.94 (kW·h) compared to the comparison model. The average battery loss of this model is 77% lower than the battery loss in the comparison model. From the aforementioned data, we can see that the values of the three objective functions after solving the FVCS-WPIES model are smaller than those of the comparison model, and the Pareto solution set of the FVCS-WPIES model dominates the Pareto solution set of the comparison model. Based on the analysis, it can be concluded that the FVCS-WPIES model is superior to the comparison model. Additionally, the FVCS strategy proposed in the paper outperforms the traditional model's average wind and PV distribution strategy. In the next step, the Pareto solution set obtained by solving the FVCS-WPIES model will be examined to further validate the model's effectiveness.

Typical solution decisions

In this paper, the EWM is used to make decisions on the Pareto solution set after solving the FVCS-WPIES model. EWM is a multi-criteria decision analysis method, based on the concept of information entropy, by calculating the entropy value and entropy weight of the criteria, to determine the weight of each criterion. The information entropy reflects the amount of information and uncertainty of each criterion, while the method takes into account the correlation between the criteria. Therefore, the entropy method can effectively exert the relationship between multiple criteria and improve the accuracy and reliability of decision making. The EWM solves the FVCS-WPIES model decision steps as follows.

(1) Indicator positive normalization.

$$x'_{ij} = \max(x_{ij}) - x_{ij} \quad \text{(Equation 33)}$$

(2) Data normalization.

$$r_{ij} = \frac{x'_{ij} - \min(x'_j)}{\max(x'_j) - \min(x'_j)} \quad \text{(Equation 34)}$$

(3) Calculating information entropy.

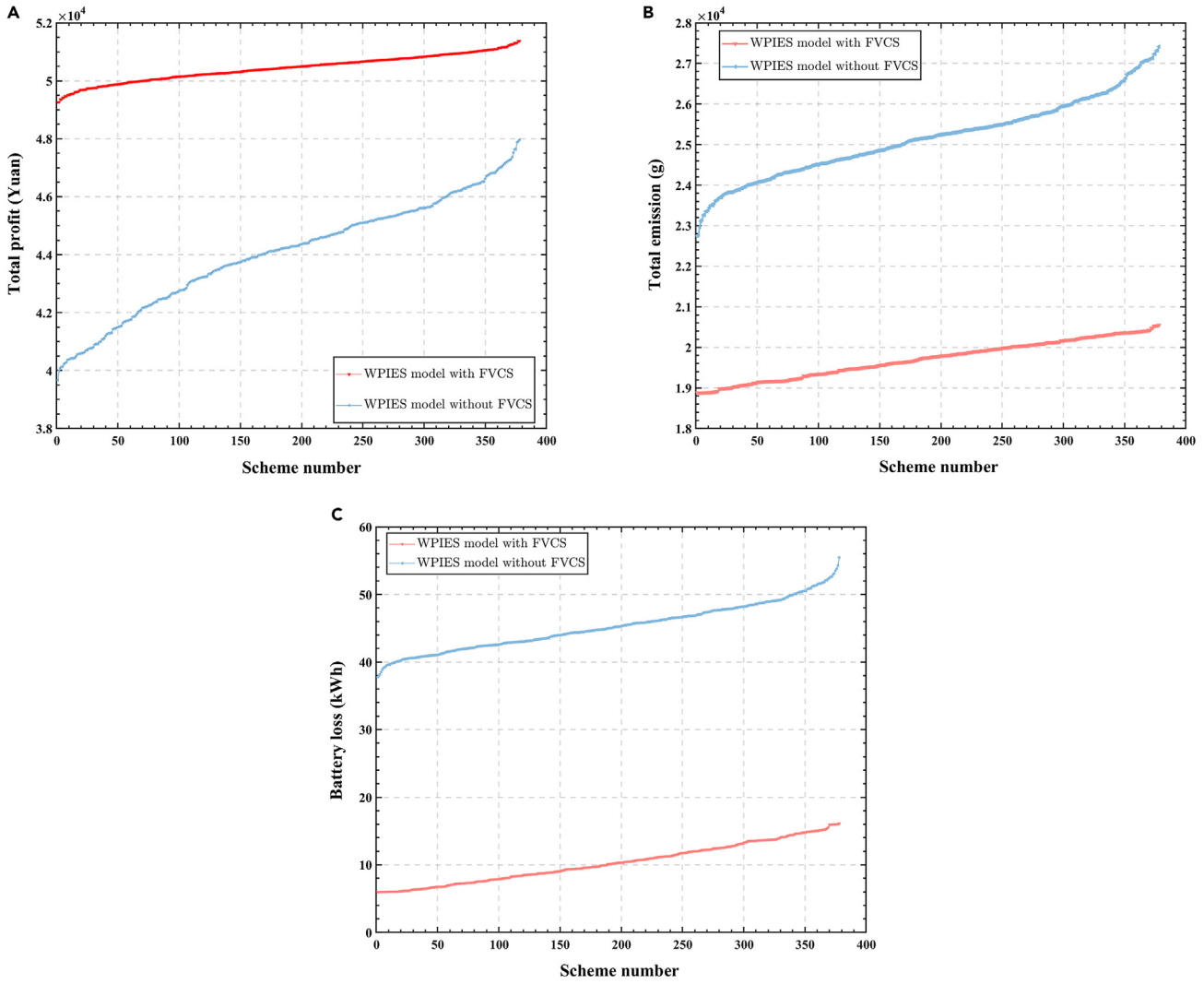

Figure 9. Two models objective functions

(A) Total profit.

(B) Total emission.

(C) Battery loss.

$$E_j = -\frac{1}{lnm}\sum_{i=1}^{m} p_{ij}\, ln\, p_{ij} \quad \text{(Equation 35)}$$

$$p_{ij} = \frac{r_{ij}}{\sum_{j=1}^{n} r_{ij}} \quad \text{(Equation 36)}$$

(4) Weighting and score calculation.

$$w_{ij} = \frac{(1 - E_j)}{\sum_{j=1}^{n} (1 - E_j)} \quad \text{(Equation 37)}$$

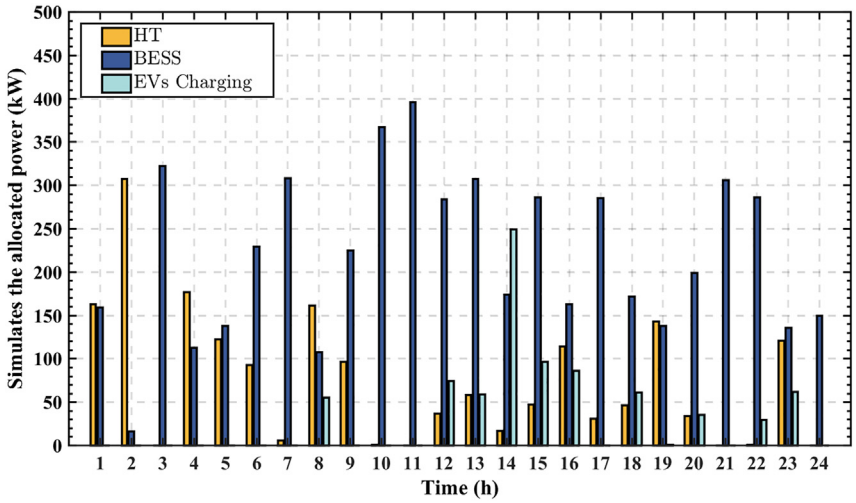

Figure 10. Pre-distribution value of wind/PV for each module of the upper-level model

$$S_i = \sum_{j=1}^{n} w_j r_{ij} \quad \text{(Equation 38)}$$

After solving by the EWM, the objective weights are [0.3599, 0.3355, 0.3046], the optimal entropy value of the decisioned scheme is 0.5922, and the optimal result objective function value is [-49881.6381, 19342.6391, 6.4026]. The result corresponds to the group 252 solution of the Pareto solution set of the FVCS-WPIES model. The objective function values for this solution are F1 (total profit) = −49881.6381, F2 (pollutant emissions) = 19342.6391, F3 (battery losses) = 6.4026. The next step will be to summarize the optimal solution decided by the entropy method, analyze the operating conditions of the solution and verify the rationality of the FVCS-WPIES model.

Typical solution analysis

This section analyzes the SOC state changes of BESS and HT, the purchased power of EV, HT, and BESS modules at each moment, the net gain of HV and EV at each moment, the charging and discharging power of the BESS system at each moment, and the wind and PV power share of each sub-module of the integrated energy station at each moment. Under the hydrogen power constraint $1 - \alpha = 99\%$, the optimization results of the 252nd solution decided by the EWM are shown in the following. Among them, Figures 10 and 11 shows the SOC state changes of the BESS and HT modules for one day, and Figure 12 shows the number of fully charged and not fully charged batteries in the BSS at each time of day. In the upper-level model, the solution result of the FVCS strategy is the pre-distribution value of the wind/PV of each module in the lower-level model. If the profit value in the solution of the lower-level model is less than the expected profit of the upper-level

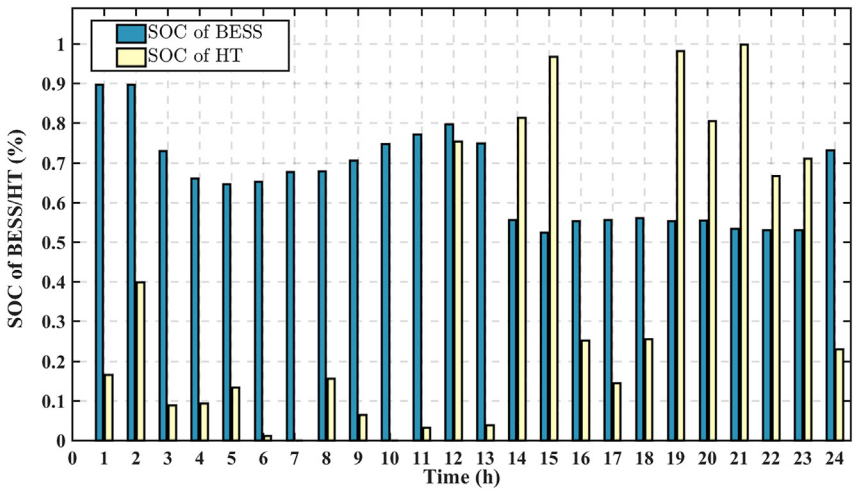

Figure 11. BCS module and HT module SOC state change diagram

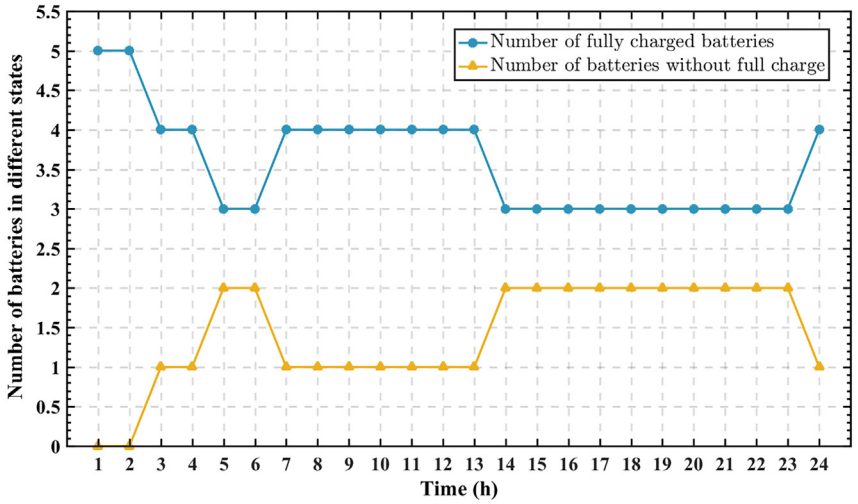

Figure 12. Number of batteries in different states of charge in the BSS module at different times

model, the penalty coefficient is increased, and the iteration and optimization are carried out again. The solution results of the upper-level model are shown in Figure 10.

Figure 13 shows the purchased electricity for HT, BESS and EV for each time of the day. It can be seen that after passing the hydrogen power constraint, in the peak hours of the TOU, only the 14:00 and 19:00 h show a large number of power purchases, and these 2 h are exactly the two moments when the HV hydrogen demand is the largest, so there will be a large number of power purchases from the HT module during the peak hours of the tariff. With the hydrogen power constraint, there is no large amount of power purchase during the remaining peak hours of 12:00–13:00, 15:00–16:00, and 20:00–21:00, which greatly reduces the cost of hydrogen production at the integrated energy station and thus increases the overall revenue. where the purchased power of the BESS module and the EV module is less than the purchased power of the HT, and thus shown in the enlarged subplot of Figure 13. Figures 14 and 15 shows the returns of EV and HV for each time period.

Figure 16 shows the charge and discharge quantities of the BESS system for each time period, i.e., the total charge and discharge quantities of all batteries in the BCS module and the BSS module for each time period, where the charge quantity is a positive number and the

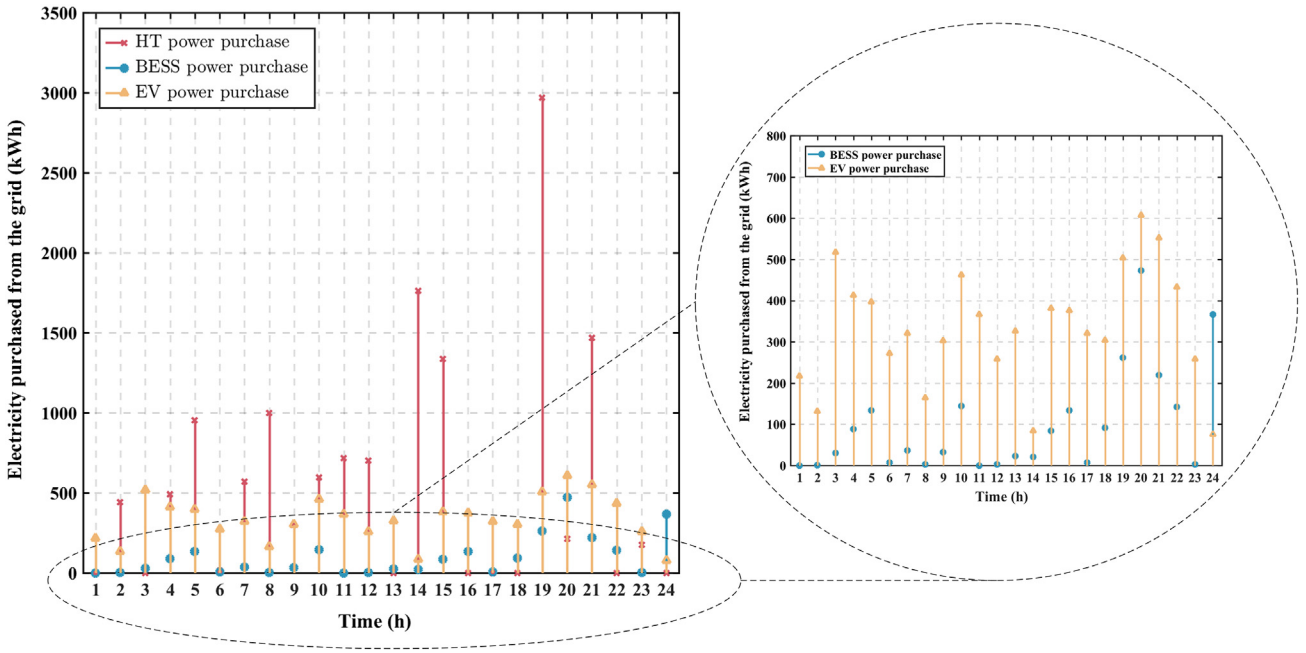

Figure 13. BESS module and EV module power purchase by time period

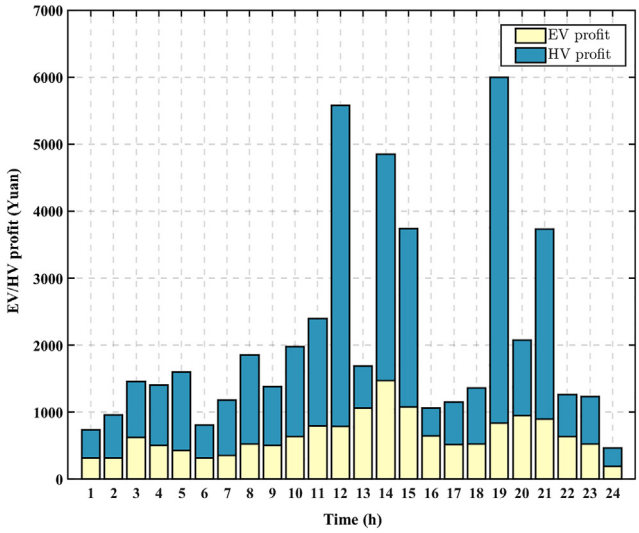

Figure 14. EV and HV earnings by time period

discharge quantity is a negative number. From the graph, we can see that during the peak hours of 13:00–16:00 and 19:00–22:00, the EV energy storage battery is overall is discharged externally, providing power to EV charging or selling to the grid, thus reducing the purchased power from the grid, reducing the operating cost of the integrated energy station and increasing the total revenue. And the graph also shows that during the low tariff hours between 3:00–6:00, the battery also has a discharge operation, the reason analysis is because the power allocated by the wind and PV is high during this time while the EV load is low during this time, so there will be a discharge phenomenon during the low tariff hours.

Figure 16 shows the percentage of wind and PV for each sub-module of the FVCS-WPIES system. As can be seen from the figure, after the WPIES bi-level optimization model with the addition of FVCS is solved by the ANSGA-III algorithm, the wind and PV is assigned to the BESS module in priority, while the part exceeding the power demand of the BESS module is assigned to the HT module in priority. However, during the peak tariff hours of 12:00–16:00, some of the wind and PV power will be provided for EV charging, thus reducing the operating costs of the integrated energy station and increasing the overall revenue. Compared with the results of the comparison model, the FVCS-WPIES model reduces the wind/PV distribution value of the BESS module, thus greatly reducing the loss of the BESS module, and therefore increasing the overall income of the integrated power station. In summary, through the analysis and demonstration in this section, it can be concluded that the optimal scheduling model of the energy system of the integrated energy station with FVCS is better than other optimal scheduling models with average distribution of wind and PV. Therefore, the rationality of the FVCS-WPIES system model proposed in this paper can be verified.

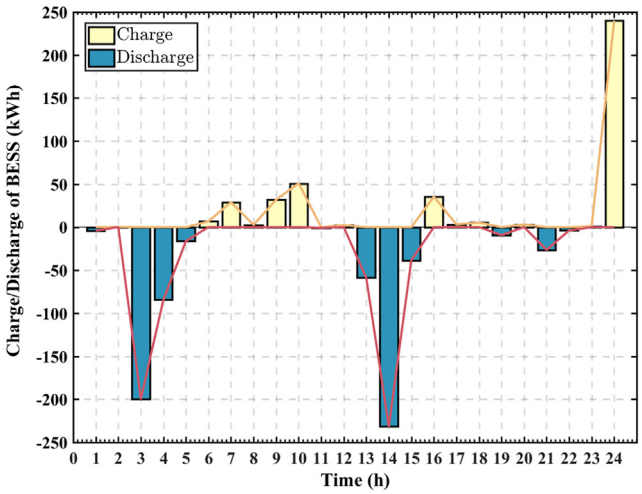

Figure 15. Total charge and discharge of BESS module by time period

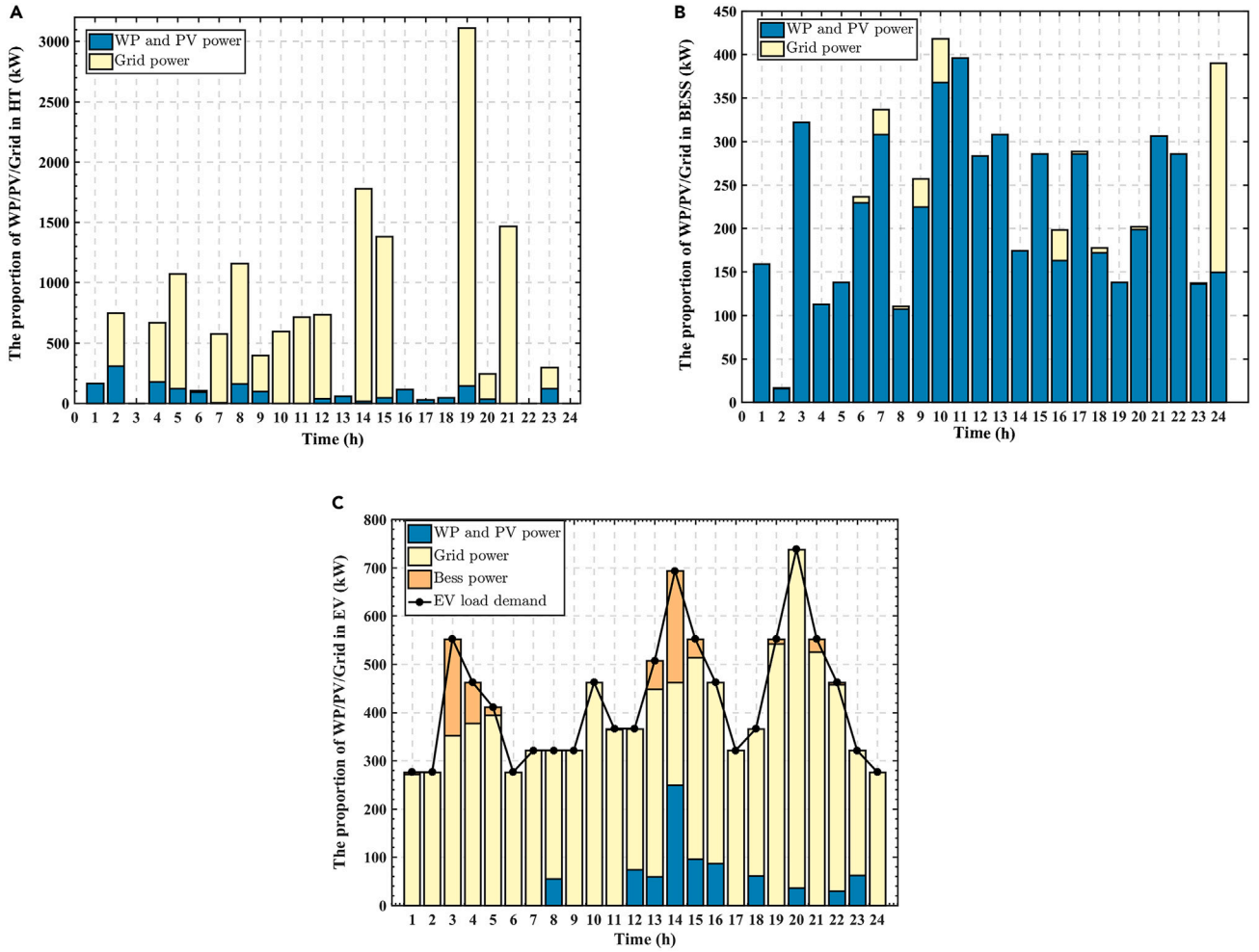

Figure 16. Wind and PV ratio of each sub-module

(A) HT module.

(B) BESS module.

(C) EV module.

Application prospects

A more accurate and complex model is needed to describe the FVCS-WPIES system in the actual operating conditions of an integrated energy station. China has started developing comprehensive energy stations by transforming traditional gas stations into facilities that also incorporate wind/PV and hydrogen storage. These stations have been put into operation. Furthermore, BESS and HRS technologies are relatively mature and have already been implemented in several places in real life. The FVCS-WPIES system model proposed in this paper can improve the efficiency of renewable energy utilization, reduce operating costs, and improve the operating life of integrated energy stations compared with the independent open large BESS and HRS technologies. Therefore, FVCS-WPIES has good use and practicality in promoting the development of electric and hydrogen vehicles in the future.

Conclusions

This paper proposes an energy management model for grid-connected FVCS-WPIES systems. The model supports the development of EV charging and swapping as well as HV. It plays a crucial role in the optimal scheduling of future energy systems in integrated energy stations. The FVCS-WPIES model has reduced operating costs, battery losses, and pollutant emissions of energy stations with wind and PV power. The FVCS-WPIES model has been compared with the conventional model of an integrated energy station with an average distribution of wind and PV power, and the model has been solved separately using the ANSGA-III algorithm. The results have indicated that the Pareto solution set solved by the FVCS-WPIES system model proposed in this study has dominated the Pareto solution set of the conventional model. Therefore, it has been concluded that the FVCS-WPIES model has been more applicable to the optimal scheduling of energy systems in integrated energy stations than the conventional model. Finally, the Pareto solution set has been determined using the EWM after solving the FVCS-WPIES

model. The 252nd solution has been selected as a typical solution for analysis, and the analysis has verified the rationality of the FVCS-WPIES model.

Limitations of the study

In future studies, the FVCS-WPIES optimization model will be improved to better integrate the actual operating conditions of the integrated energy station. The FVCS model will heavily depend on actual data and forecasts of wind and PV power generation. Therefore, planning studies will be required to obtain actual data from integrated energy stations. The uncertainty of the demand of wind/PV and car users will largely affect the day-ahead optimal scheduling of the integrated energy station, so the robustness optimization of the model will also be an important research element in the future. Finally, neural networks and deep learning will be combined with many-objective optimization algorithms to improve the solving efficiency of the model, solve the real-time decision-making problem, and realize the real-time adjustment of the day-ahead scheduling.

STAR★METHODS

Detailed methods are provided in the online version of this paper and include the following:

- KEY RESOURCES TABLE
- RESOURCE AVAILABILITY
  - Lead contact
  - Materials availability
  - Data and code availability
- METHOD DETAILS
  - Future Value Competition Strategy
  - Upper-level model objective function
  - Lower-level models

ACKNOWLEDGMENTS

This work is supported by the National Natural Science Foundation of China (51809097), Open Foundation of Hubei Key Laboratory for High-efficiency Utilization of Solar Energy and Operation Control of Energy Storage System (HBSEES202312), and the Open Foundation of Hubei Engineering Research Center for Safety Monitoring of New Energy and Power Grid Equipment (HBSKF202125).

AUTHOR CONTRIBUTIONS

X.L. proposed the idea and design of this study and received funding. J.M. was responsible for the execution of the experiment as well as the writing and revision of the paper. B.Y. is responsible for data collection and collation. B.Q. is responsible for data analysis and interpretation. R.L. is responsible for literature research and collation. F.B. provides analytical tools and techniques. C.L. was responsible for supervision and management, reviewed the manuscript and proposed suggestions for improvement.

DECLARATION OF INTERESTS

The authors declare no competing interests.

Received: October 24, 2023
Revised: January 18, 2024
Accepted: February 16, 2024
Published: February 23, 2024

REFERENCES

1. Li, Y., Cai, Y., Zhao, T., Liu, Y., Wang, J., Wu, L., and Zhao, Y. (2022). Multi-objective Optimal Operation of Centralized Battery Swap Charging System with Photovoltaic. J. Mod. Power Syst. Clean Energy *10*, 149–162. https://doi.org/10.35833/mpce.2020.000109.
2. Ban, M.F., Yu, J.L., and Yao, Y.Y. (2021). Joint Optimal Scheduling for Electric Vehicle Battery Swapping-charging Systems Based on Wind Farms. CSEE J. Power Energy Syst. *7*, 555–566. https://doi.org/10.17775/cseejpes.2020.02380.
3. Yuan, H., Wei, G., Zhu, L., Zhang, X., Zhang, H., Luo, Z., and Hu, J. (2020). Optimal scheduling for micro-grid considering EV charging-swapping-storage integrated station. IET Gener. Transm. Distrib. *14*, 1127–1137. https://doi.org/10.1049/iet-gtd.2018.6912.
4. Tao, Y., Qiu, J., Lai, S., Sun, X., Zhao, J., Zhou, B., and Cheng, L. (2022). Data-driven on-demand energy supplement planning for electric vehicles considering multi-charging/swapping services. Appl. Energy *311*, 118632. https://doi.org/10.1016/j.apenergy.2022.118632.
5. Zaher, G.K., Shaaban, M.F., Mokhtar, M., and Zeineldin, H.H. (2021). Optimal operation of battery exchange stations for electric vehicles. Elec. Power Syst. Res. *192*, 106935. https://doi.org/10.1016/j.epsr.2020.106935.
6. Wang, Y., Lai, K., Chen, F., Li, Z., and Hu, C. (2019). Shadow price based co-ordination methods of microgrids and battery swapping stations. Appl. Energy *253*, 113510. https://doi.org/10.1016/j.apenergy.2019.113510.
7. Gong, D., Tang, M., Liu, S., Xue, G., and Wang, L. (2019). Achieving sustainable transport through resource scheduling: A case study for electric vehicle charging stations. Adv. produc. engineer. manag. *14*,

65–79. https://doi.org/10.14743/apem2019.1.312.
8. Zhang, Y., You, P., and Cai, L. (2019). Optimal Charging Scheduling by Pricing for EV Charging Station With Dual Charging Modes. IEEE trans. Intell. Transp. Syst. *20*, 3386–3396. https://doi.org/10.1109/tits.2018.2876287.
9. Leou, R.C., and Hung, J.J. (2017). Optimal Charging Schedule Planning and Economic Analysis for Electric Bus Charging Stations. Energies *10*, 483. https://doi.org/10.3390/en10040483.
10. Al-Hanahi, B., Ahmad, I., Habibi, D., Pradhan, P., and Masoum, M.A.S. (2022). An Optimal Charging Solution for Commercial Electric Vehicles. IEEE Access *10*, 46162–46175. https://doi.org/10.1109/access.2022.3171048.
11. Song, Y., Zheng, Y., and Hill, D. (2016). Optimal Scheduling for EV Charging Stations in Distribution Networks: A Convexified Model. IEEE Trans. Power Syst. *32*, 1–1575. https://doi.org/10.1109/tpwrs.2016.2568746.
12. Das, R., Wang, Y., Putrus, G., Kotter, R., Marzband, M., Herteleer, B., and Warmerdam, J. (2020). Multi-objective techno-economic-environmental optimisation of electric vehicle for energy services. Appl. Energy *257*, 113965. https://doi.org/10.1016/j.apenergy.2019.113965.
13. Sun, B. (2021). A multi-objective optimization model for fast electric vehicle charging stations with wind, PV power and energy storage. J. Clean. Prod. *288*, 125564. https://doi.org/10.1016/j.jclepro.2020.125564.
14. Çiçek, A. (2022). Optimal operation of an all-in-one EV station with photovoltaic system including charging, battery swapping and hydrogen refueling. Int. J. Hydrogen Energy *47*, 32405–32424. https://doi.org/10.1016/j.ijhydene.2022.07.171.
15. Bilal, M., Ahmad, F., and Rizwan, M. (2023). Techno-economic assessment of grid and renewable powered electric vehicle charging stations in India using a modified metaheuristic technique. Energy Convers. Manag. *284*, 116995. https://doi.org/10.1016/j.enconman.2023.116995.
16. Ahmadi Jirdehi, M., and Sohrabi Tabar, V. (2023). Risk-aware energy management of a microgrid integrated with battery charging and swapping stations in the presence of renewable resources high penetration, crypto-currency miners and responsive loads. Energy *263*, 125719. https://doi.org/10.1016/j.energy.2022.125719.
17. Zou, J., Shu, J., Zhang, Z., and Luo, W. (2014). An Active Power Allocation Method for Wind-solar-batteries Hybrid Power System. Elec. Power Compon. Syst. *42*, 1530–1540. https://doi.org/10.1080/15325008.2014.943434.
18. Nehrir, M.H., Wang, C., Strunz, K., Aki, H., Ramakumar, R., Bing, J., Miao, Z., and Salameh, Z. (2011). A Review of Hybrid Renewable/Alternative Energy Systems for Electric Power Generation: Configurations, Control, and Applications. IEEE Trans. Sustain. Energy *2*, 392–403. https://doi.org/10.1109/tste.2011.2157540.
19. Datta, M., Senjyu, T., Yona, A., and Funabashi, T. (2011). Photovoltaic Output Power Fluctuations Smoothing by Selecting Optimal Capacity of Battery for a Photovoltaic-Diesel Hybrid System. Elec. Power Compon. Syst. *39*, 621–644. https://doi.org/10.1080/15325008.2010.536809.
20. Meiqin, M., Meihong, J., Wei, D., and Chang, L. (2010). Multi-objective Economic Dispatch Model for a Microgrid Considering Reliability, pp. 993–998.
21. Jain, H., and Deb, K. (2014). An Evolutionary Many-Objective Optimization Algorithm Using Reference-Point Based Nondominated Sorting Approach, Part II: Handling Constraints and Extending to an Adaptive Approach. IEEE Trans. Evol. Comput. *18*, 602–622. https://doi.org/10.1109/tevc.2013.2281534.
22. Saner, C.B., Trivedi, A., and Srinivasan, D. (2022). A Cooperative Hierarchical Multi-Agent System for EV Charging Scheduling in Presence of Multiple Charging Stations. IEEE Trans. Smart Grid *13*, 2218–2233. https://doi.org/10.1109/tsg.2022.3140927.
23. Su, S., Wei, C., Li, Z., Xia, M., and Chen, Q. (2022). Critical load restoration in coupled power distribution and traffic networks considering spatio-temporal scheduling of electric vehicles. Int. J. Electr. Power Energy Syst. *141*, 108180. https://doi.org/10.1016/j.ijepes.2022.108180.
24. Wu, Z., and Chen, B. (2021). Distributed Electric Vehicle Charging Scheduling with Transactive Energy Management. Energies *15*, 163. https://doi.org/10.3390/en15010163.
25. Dai, Q., Liu, J., and Wei, Q. (2019). Optimal Photovoltaic/Battery Energy Storage/Electric Vehicle Charging Station Design Based on Multi-Agent Particle Swarm Optimization Algorithm. Sustainability *11*, 1973. https://doi.org/10.3390/su11071973.
26. Zhang, X., and Zheng, L. (2019). Coordinated dispatch of the wind-thermal power system by optimizing electric vehicle charging. Cluster Comput. *22*, S8835–S8845. https://doi.org/10.1007/s10586-018-1974-9.
27. Hao, Y., Dong, L., Liang, J., Liao, X., Wang, L., and Shi, L. (2020). Power forecasting-based coordination dispatch of PV power generation and electric vehicles charging in microgrid. Renew. Energy *155*, 1191–1210. https://doi.org/10.1016/j.renene.2020.03.169.
28. Shojaabadi, S., Talavat, V., and Galvani, S. (2022). A game theory-based price bidding strategy for electric vehicle aggregators in the presence of wind power producers. Renew. Energy *193*, 407–417. https://doi.org/10.1016/j.renene.2022.04.163.
29. Dukpa, A., and Butrylo, B. (2022). MILP-Based Profit Maximization of Electric Vehicle Charging Station Based on Solar and EV Arrival Forecasts. Energies *15*, 5760. https://doi.org/10.3390/en15155760.
30. Amiri, S.S., Jadid, S., and Saboori, H. (2018). Multi-objective optimum charging management of electric vehicles through battery swapping stations. Energy *165*, 549–562. https://doi.org/10.1016/j.energy.2018.09.167.
31. Shi, R., Zhang, P., Zhang, J., Niu, L., and Han, X. (2020). Multidispatch for Microgrid including Renewable Energy and Electric Vehicles with Robust Optimization Algorithm. Energies *13*, 2813. https://doi.org/10.3390/en13112813.
32. Wen, L., Zhou, K., Yang, S., and Lu, X. (2019). Optimal load dispatch of community microgrid with deep learning based solar power and load forecasting. Energy *171*, 1053–1065. https://doi.org/10.1016/j.energy.2019.01.075.
33. Xu, X., Hu, W., Liu, W., Du, Y., Huang, Q., and Chen, Z. (2022). Robust energy management for an on-grid hybrid hydrogen refueling and battery swapping station based on renewable energy. J. Clean. Prod. *331*, 129954. https://doi.org/10.1016/j.jclepro.2021.129954.
34. Xu, X., Hu, W., Cao, D., Huang, Q., Chen, C., and Chen, Z. (2020). Optimized sizing of a standalone PV-wind-hydropower station with pumped-storage installation hybrid energy system. Renew. Energy *147*, 1418–1431. https://doi.org/10.1016/j.renene.2019.09.099.
35. Gökmen, N., Hu, W., Hou, P., Chen, Z., Sera, D., and Spataru, S. (2016). Investigation of wind speed cooling effect on PV panels in windy locations. Renew. Energy *90*, 283–290. https://doi.org/10.1016/j.renene.2016.01.017.
36. Micena, R.P., Llerena-Pizarro, O.R., de Souza, T.M., and Silveira, J.L. (2020). Solar-powered Hydrogen Refueling Stations: A techno-economic analysis. Int. J. Hydrogen Energy *45*, 2308–2318. https://doi.org/10.1016/j.ijhydene.2019.11.092.
37. Li, C.-H., Zhu, X.-J., Cao, G.-Y., Sui, S., and Hu, M.-R. (2009). Dynamic modeling and sizing optimization of stand-alone photovoltaic power systems using hybrid energy storage technology. Renew. Energy *34*, 815–826. https://doi.org/10.1016/j.renene.2008.04.018.
38. Dey, B., Basak, S., and Bhattacharyya, B. (2023). Demand-Side-Management-Based Bi-level Intelligent Optimal Approach for Cost-Centric Energy Management of a Microgrid System. Arab. J. Sci. Eng. *48*, 6819–6830. https://doi.org/10.1007/s13369-022-07546-2.
39. Dey, B., Misra, S., and Garcia Marquez, F.P. (2023). Microgrid system energy management with demand response program for clean and economical operation. Appl. Energy *334*, 120717. https://doi.org/10.1016/j.apenergy.2023.120717.
40. Chhualsingh, T., Rao, K.S., Rajesh, P.S., and Dey, B. (2023). Effective demand response program addresing carbon constrained economic dispatch problem of a microgrid system. e-Prime *5*, 100238. https://doi.org/10.1016/j.prime.2023.100238.
41. Qu, C., He, W., Peng, X., and Peng, X. (2020). Harris Hawks optimization with information exchange. Appl. Math. Model. *84*, 52–75. https://doi.org/10.1016/j.apm.2020.03.024.
42. Farzin, H., Fotuhi-Firuzabad, M., and Moeini-Aghtaie, M. (2016). A Practical Scheme to Involve Degradation Cost of Lithium-Ion Batteries in Vehicle-to-Grid Applications. IEEE Trans. Sustain. Energy *7*, 1730–1738. https://doi.org/10.1109/tste.2016.2558500.
43. Guo, L., Liu, W., Jiao, B., Hong, B., and Wang, C. (2014). Multi-objective stochastic optimal planning method for stand-alone microgrid system. IET Gener. Trans. Distrib. *8*, 1263–1273. https://doi.org/10.1049/iet-gtd.2013.0541.

STAR★METHODS

KEY RESOURCES TABLE

REAGENT or RESOURCE	SOURCE	IDENTIFIER
Deposited data		
Wind power and PV power	Sun[13]	https://doi.org/10.1016/j.jclepro.2020.125564
Wind turbine data	Xu et al.[34]	https://doi.org/10.1016/j.renene.2019.09.099
Hydrogen production data	Li et al.[37]	http://doi.org/10.1016/j.renene.2008.04.018
Battery loss	Farzin et al.[42]	https://ieeexplore.ieee.org/document/7514958
Emission data of air pollutants by power generation type	Ministry of Ecology and Environment of the People's Republic of China	https://www.mee.gov.cn/ywgz/fgbz/bz/bzwb/dqhjbh/dqgdwrywrwpfbz/
Software and algorithms		
MatlabR2021b	MathWorks.Inc	https://ww2.mathworks.cn/
Upper-level model code	This paper	https://github.com/MMAJUN/Model
Lower-level Model code	This paper	https://github.com/MMAJUN/Model

RESOURCE AVAILABILITY

Lead contact

Further information and requests for resources should be directed to and will be fulfilled by the lead contact, Jun Ma (ma.jun@hbut.edu.cn).

Materials availability

This study did not generate new unique reagents.

Data and code availability

- All data reported in this paper will be shared by the lead contact upon request.
- All original code has been deposited at Github and is publicly available as of the date of publication. DOI is listed in the key resources table.
- Any additional information required to reanalyse the data reported in this paper is available from the lead contact upon request.

METHOD DETAILS

Future Value Competition Strategy

In the upper-level model, PV and wind power are allocated to the EV charging module, hydrogen production module, and battery storage system module respectively through a FVCS. Under the background of TOU, the operation and control conditions of the energy system of the integrated energy station will change with the different power of PV and wind power generation at different times, and the benefits generated will be different. Therefore, the FVCS proposed in this paper changes the previous wind and PV system power distribution in an average way. The allocation of the active power of the wind and PV in the integrated energy station is controlled by the wind and PV energy allocation strategy based on target optimization, thus changing the energy share of each subsystem in the integrated energy station. In the optimization process of the lower-level model (WPIES), the distribution value of wind/PV of each module is random, which affects the electricity purchased by each module from the grid at each moment, and finally affects the overall income of the integrated energy station. The upper-level model (FVCS) was used for pre-distribution to solve the power allocation scheme with the maximum total return. After solving the WPIES model, the return objective function was compared with FVCS in order to enhance the active power distribution value of wind/PV and improve the optimization outcome of the FVCS-WPIES model. The principle of FVCS is illustrated in Figure 7.

FVCS calculates the distribution of active power from the wind and PV system to each subsystem by measuring the expected benefit of the energy generated by the wind and PV flowing into each subsystem of the integrated energy station and solves the optimization model using the Harris Hawks algorithm (HHO).

To enhance the accuracy of the upper-level model, penalty functions are added to it. Once the lower-level model is resolved, if the actual operating conditions during time period t fail to achieve the anticipated profit, the objective function value of the upper-level model is penalized. The penalty function can be expressed in the following manner.

$$\sum_{i=1}^{m} \omega_i \max\{0, x_1 - x_2\} \quad \text{(Equation 39)}$$

where ω_i denotes the penalty weight. x_1 denotes the value of the optimized objective function, i.e., the expected profit. x_2 denotes the actual profit after optimization of the lower-level model.

Upper-level model objective function

The objective function of the upper-level model is to maximize the expected profit. Electricity allocated to the hydrogen production module is converted into hydrogen for HV hydrogenation, and the electricity allocated to the BESS module is sold to the grid. The expected profit objective function of the upper-level model is shown in Equation 40.

$$\max F_{profit}^{FVCS} = \sum_{t=1}^{T} W_t^{BESS,WP} \times P_{discharge,t}^{price} + W_t^{EV,WP} \times P_{sell,t}^{price} + W_t^{HT,WP} \times \eta_{H_2} \times P_{H_2}^{price} \quad \text{(Equation 40)}$$

where $W_t^{BESS,WP}$ is the amount of power allocated to BESS through FVCS in time period t. $P_{discharge,t}^{price}$ is the price of electricity sold to the grid in time period t. $W_t^{EV,WP}$ is the amount of power allocated to the EV charging module via FVCS in time period t. $P_{sell,t}^{price}$ is the price of EV charging at time t. $W_t^{HT,WP}$ is the amount of power allocated to the hydrogen production module through FVCS in time t. $P_{H_2}^{price}$ is the price of selling hydrogen. η_{H_2} is the efficiency of converting electricity to hydrogen.

The objective function of the upper-level model is to maximize the expected profit. Electricity allocated to the hydrogen production module is converted into hydrogen for HV hydrogenation, and the electricity allocated to the BESS module is sold to the grid. The expected profit objective function of the upper-level model is shown in Equation 41.

$$\max F_{profit}^{FVCS} = \sum_{t=1}^{T} W_t^{BESS,WP} \times P_{discharge,t}^{price} + W_t^{EV,WP} \times P_{sell,t}^{price} + W_t^{HT,WP} \times \eta_{H_2} \times P_{H_2}^{price} \quad \text{(Equation 41)}$$

where $W_t^{BESS,WP}$ is the amount of power allocated to BESS through FVCS in time period t. $P_{discharge,t}^{price}$ is the price of electricity sold to the grid in time period t. $W_t^{EV,WP}$ is the amount of power allocated to the EV charging module via FVCS in time period t. $P_{sell,t}^{price}$ is the price of EV charging at time t. $W_t^{HT,WP}$ is the amount of power allocated to the hydrogen production module through FVCS in time t. $P_{H_2}^{price}$ is the price of selling hydrogen. η_{H_2} is the efficiency of converting electricity to hydrogen.

Lower-level models

This section presents the economic, operational and environmental objectives pursued for the optimal operation of integrated energy stations. At the core of the lower-level model energy management are three objective functions, consisting of maximizing total revenue, minimizing battery losses and minimizing pollutant emissions, respectively.

From the perspective of the operation of an integrated energy station, the total profit of a station is a fundamental goal. Energy management of EVs, hydrogen vehicles and the power grid based on TOU can maximize the operational benefits of integrated energy stations. In this study, the total profit objective function of the integrated energizing station is shown as flows. The algorithm in the code solves for the minimum value of the objective function. Therefore, we take the negative of the total profit objective function in the code to obtain the minimum value as the result.

$$\max F_{profit}^{WPIES} = f_{profit}^{BCS} + f_{profit}^{BSS} + f_{profit}^{EV} + f_{profit}^{HT} \quad \text{(Equation 42)}$$

$$W_t^{BESS,WP} = W_t^{BCS,WP} + W_t^{BSS,WP} \quad \text{(Equation 43)}$$

$$\begin{cases} f_{profit}^{BCS} = \sum_{t=1}^{T} P_{discharge,t}^{BCS} \times \Delta t_2 \times P_{discharge,t}^{price} - \left(P_{charge,t}^{BCS} \times \Delta t_1 - W_t^{BCS,WP}\right) \times P_{buy,t}^{price} \\ f_{profit}^{BSS} = \sum_{t=1}^{T} \left[0.9 C_{Battery} \times N_t^{EV,BSS} \times P_{sell,t}^{price} - \left(W_t^{BSS} - W_t^{BSS,WP}\right) \times P_{buy,t}^{price}\right] \\ f_{profit}^{EV} = \sum_{t=1}^{T} P_{charge,t}^{EV} \times \Delta t_2 \times P_{sell,t}^{price} - W_{charge,t}^{EV} \times P_{buy,t}^{price} \\ f_{profit}^{HT} = \sum_{t=1}^{T} Q_t^{HV} \times P_{H_2}^{price} - \left(\frac{\Delta SOC_{t,t-1}^{HT} \times C_{HT}}{\eta_{H_2}} - W_t^{HT,WP}\right) \times P_{buy,t}^{price} \end{cases} \quad \text{(Equation 44)}$$

where $P_{discharge,t}^{BCS}$ and $P_{charge,t}^{BCS}$ are divided into the discharging power and charging power of BCS at time t. $P_{buy,t}^{price}$ is divided into the price of electricity purchased from the grid in time t. $P_{charge,t}^{EV}$ is the charging power of EV at time t. $W_{charge,t}^{EV}$ is the amount of electricity purchased from

the grid by the EV charging module at time t. Q_t^{HV} is the weight of hydrogen required for HVs in time period t. $\Delta SOC_{t,t-1}^{HT}$ is the change in hydrogen SOC of HT in time t and time t-1.

Reducing the battery storage system of integrated energy station can effectively increase the operating life of integrated energy station. The main factors of battery wear are related to the number of cycles, operating temperature, charging and discharging efficiency, DOD, SOC and end-of-charge voltage (EOCV) [42]. Therefore, in the WPIES model, the wear factor (kW·h/kW·h) for Li-ion batteries with the same ACC-DOD characteristics. This value is mainly related to the change in total battery energy. Ignoring other factors in this application. In this study, the minimum objective function of the loss of the BESS in the integrated energy station is shown as follows.

$$\min F_{loss}^{WPIES} = K_w \sum_{t=1}^{T} P_{charge,t}^{BCS} \times \Delta t_1 + P_{discharge,t}^{BCS} \times \Delta t_2 + W_t^{BSS} \quad \text{(Equation 45)}$$

Where $K_w = 0.00015\text{kW}\bullet\text{h}$. This means that each kW·h of charging or discharging of the EV battery will reduce the available energy of the Li-ion battery by approximately 0.00015 kW h.

Application of the WPIES model will positively reduce global carbon emissions. The load of the integrated energy station is mainly provided by wind power and PV power generation. In this study, the environmental pollution emissions from the integrated energy station are mainly caused by the electricity purchased from the grid. Therefore, the objective function is to minimize the emissions of SO_2, NO_x and CO_2. The objective function is as follows.

$$\min F_{CO_2,SO_2,NO_x}^{WPIES} = \sum_{t=1}^{T} W_{buy,t}^{Grid} \times \left(e_{CO_2} + e_{SO_2} + e_{NO_x}\right) \quad \text{(Equation 46)}$$

$$W_{buy,t}^{Grid} = P_{charge,t}^{BCS} \times \Delta t_1 + W_t^{BSS} + W_{charge,t}^{EV} + \frac{\Delta SOC_{t,t-1}^{HT} \times C_{HT}}{\eta_{H_2}} - W_t^{WP} \quad \text{(Equation 47)}$$

where $W_{buy,t}^{Grid}$ is the amount of electricity purchased from the grid by WPIES in time period t. e_{CO_2}, e_{SO_2} and e_{NO_x} are the emission factors of SO_2, NO_x and CO_2 per kW·h from the utility grid, respectively. W_t^{WP} is the amount of wind and PV power generated at time t.